Available online at www.sciencedirect.com
ScienceDirect
Deep-Sea Research I 54 (2007) 1815–1840
DEEP-SEA RESEARCH PART I
www.elsevier.com/locate/dsri

Northwestern Weddell Sea deep outflow into the Scotia Sea during the austral summers of 2000 and 2001 estimated by inverse methods

Bárbara C. Franco[a,*], Mauricio M. Mata[a], Alberto R. Piola[b,c], Carlos A.E. Garcia[a]

[a]Departamento de Física, Fundação Universidade Federal do Rio Grande, Caixa Postal 474, 96201-900 Rio Grande, RS, Brazil
[b]Departamento Oceanografía, Servicio de Hidrografía Naval, Av. Montes de Oca 2124, C1270ABV Buenos Aires, Argentine
[c]Departamento de Ciencias de la Atmósfera y los Océanos, FCEN, Universidad de Buenos Aires, Buenos Aires, Argentine

Received 23 October 2006; received in revised form 14 June 2007; accepted 20 June 2007
Available online 26 June 2007

Abstract

The northward outflow of cold, dense water from the Weddell Sea into the world ocean basins plays a key role in balancing the global heat budget. We estimate the geostrophic flow patterns in the northwestern Weddell Sea using box inverse methods applied to quasi-synoptic hydrographic data collected during the Brazilian DOVETAIL 2000 and 2001 austral summer cruises. The analysis is focused on the variations of the deep Weddell Sea outflow into the Scotia Sea within boxes that bound the main deep gaps over the South Scotia Ridge. To determine the geostrophic volume transports in each box, mass, salt, and heat are conserved within neutral density layers that are not in contact with the atmosphere. Implementing the inverse model and using property anomaly equations weighted by the flow estimate uncertainty our results are consistent with those reported in the literature. A bottom triangle extrapolation method is introduced, which improves the estimated property fluxes through hydrographic sections. In the austral summer of 2000 the transports of Weddell Sea Deep Water (WSDW) through the Philip Passage, Orkney Passage, and southwestern Bruce Passage are 0.01 ± 0.01, 1.15 ± 0.33, and 1.03 ± 0.23 Sv (1 Sv $= 10^6\,\mathrm{m^3\,s^{-1}}$, >0 is northward), respectively. After extrapolation within bottom triangles these transports increase to 0.12 ± 0.03, 3.48 ± 1.81, and 1.20 ± 2.16 Sv. Analysis of the hydrographic data reveal distinct oceanographic conditions over the Philip Passage region, with evidence of mesoscale meanders, warmer and saltier Warm Deep Water (WDW) and colder WSDW observed in 2001 than in 2000. Despite these differences the WSDW transport does not present a significant variation between 2000 and 2001. The WSDW transports through the Philip Passage in 2001 are 0.012 ± 0.001 and 0.113 ± 0.001 Sv after extrapolation within bottom triangles. The circulation derived from the inversion in the austral summer of 2001 suggests a sharp weakening of the barotropic cyclonic flow in the Powell Basin, which may be due to northerly and northeasterly winds associated with an atmospheric low-pressure center located west of the Antarctic Peninsula. We suggest that similar variations in atmospheric forcing may explain changes in the intensity of the cyclonic flow observed in the northwestern Weddell Sea and Powell Basin.
© 2007 Elsevier Ltd. All rights reserved.

Keywords: Northwestern weddell sea; Weddell sea deep water; Inverse methods; DOVETAIL; Deep outflow variations

*Corresponding author. Departamento Oceanografía, Servicio de Hidrografía Naval, Av. Montes de Oca 2124, C1270ABV, Buenos Aires, Argentina. Tel.: +54 11 43012590.
E-mail address: ocebcf@furg.br (B.C. Franco).

0967-0637/$ - see front matter © 2007 Elsevier Ltd. All rights reserved.
doi:10.1016/j.dsr.2007.06.003

1. Introduction

The Antarctic region represents an important scientific record of past climate and its variations through the evolutionary history of the Earth. Formation, sinking, and northward transport of deep and bottom waters in the Southern Ocean play a key role in the global thermohaline circulation. Dense waters originating in the Southern Ocean spread in the ocean basins further north and contribute to the global heat and freshwater budgets. Recent studies suggest that part of the dense outflow exported from the Weddell Sea into the Scotia Sea upwells because of the high turbulence in this region, which acts as a 'blender' to mix ocean water masses. As the Scotia Sea may be a significant contributor to the 'missing mixing' required to balance the global ocean overturning circulation (e.g. Heywood et al., 2002), it is important to better quantify how much dense deep water enters the basin through the South Scotia Ridge, which separates the Weddell Sea from the Scotia Sea. In addition, improved estimates of the northward transport of deep Southern Ocean waters will lead to a better understanding of global climate and its variability.

Antarctic Bottom Water (AABW, $\theta < 0\,^{\circ}C$) is the densest water mass associated with the thermohaline circulation of the world ocean (Orsi et al., 1999). AABW is produced in the southwestern and western Weddell Sea in the Atlantic sector and in the Enderby Land coast and the western Ross Sea in the Indian–Pacific sector (Whitworth et al., 1998). Based on the oceanic chlorofluoro-carbon budget, Orsi et al. (1999) diagnosed that 60% of the circumpolar production of AABW occurs in the Atlantic sector. Several studies suggest that the deep outflows from the Weddell Sea represent the most important contributions to the ventilation of the oceans (Deacon, 1933; Reid and Lynn, 1971; Mantyla and Reid, 1983; Yaremchuk et al., 1998; Schröder and Fahrbach, 1999; Muench and Hellmer, 2002). However, recent studies suggest that the Ross Sea and Adélie Land coast are also significant regions of AABW formation, possibly as large as the Weddell Sea (Rintoul, 1998; Bindoff et al., 2000).

Several studies attempted to map the outflow routes of the deep and bottom waters formed in the Weddell Sea and to quantify the transports that connect the Weddell Sea to the world ocean basins (see Rintoul, 1991; Locarnini et al., 1993; Orsi et al., 1999; Gordon et al., 2001; Naveira Garabato et al., 2002a, b; Matano et al., 2002; Schodlok et al., 2002). Estimates of Weddell Sea Deep Water (WSDW) outflow from the Weddell Sea through the South Scotia Ridge are 6.7 ± 1.7, 4.7 ± 0.7, and 6.4 Sv ($1\,Sv = 10^6\,m^3\,s^{-1}$, e.g. Naveira Garabato et al., 2002a; Schodlok et al., 2002). The bulk of these transports (4.3 ± 0.6, 5.6 ± 0.1 and 4.2 Sv, respectively) occur through the Orkney Passage, which is the deepest gap on the ridge. Nevertheless, deep water outflow estimates through some of the main deep gaps of the ridge present a wide range of variation. For instance, WSDW outflow estimates through the Philip Passage are 0.7 ± 0.4, -0.1 ± 0.3, and 2.2 Sv (e.g. Naveira Garabato et al., 2002a; Schodlok et al., 2002). These discrepancies can be attributed to sampling differences, methodologies of flow analysis, or real-time variability. Robertson et al. (2002) pointed out that the warming trend of WSDW, in recent decades is comparable to the global averaged surface-water warming (Levitus et al., 2000). Their study suggests that the deep water warming in the Weddell Sea has important implications for AABW formation, pack ice melting, regional ocean–atmosphere heat transfer, and the global thermohaline circulation. Given the differences in transport estimates through the South Scotia Ridge and the reported variations in water-mass properties in the Weddell Sea (Fahrbach et al., 1998; Robertson et al., 2002; Schröder et al., 2002), we wish to further investigate the deep outflow through the ridge and its associated variability.

The oceanographic conditions of the Weddell Sea were the focus of several international programs carried out during the 1980s and 1990s (Gordon and Huber, 1984; Fahrbach et al., 1994; Gammelsröd et al., 1994). The Deep Ocean Ventilation Through Antarctic Intermediate Layers (DOVETAIL) Program (Muench and Hellmer, 2002) was designed to map the routes and quantify the rates of deep and bottom waters recently ventilated in the Weddell Sea and exported across the Weddell–Scotia Confluence. As part of the Brazilian contribution to DOVETAIL, two cruises were conducted during the austral summers of 2000 and 2001 focused on monitoring the variability of the thermohaline structure in the northwestern Weddell Sea. This work aims to describe the water mass characteristics and circulation and to estimate the outflow of deep waters through the main deep gaps of the South Scotia Ridge during summer 2000 and 2001. It provides the first snapshots of these deep

geostrophic transports from two subsequent summers based on quasi-synoptic observations.

2. Weddell Sea general oceanography

The large-scale circulation in the Weddell Sea is dominated by the cyclonic Weddell Gyre (WG), the largest subpolar cyclonic circulation in the Southern Ocean. Circumpolar Deep Water (CDW) flowing within the Antarctic Circumpolar Current (ACC) is entrained into the WG near a broad bathymetric discontinuity in the Southwest Indian Ridge located between 25 and 32°E (Orsi et al., 1993). After entering the WG, CDW is transported westward near the Antarctic continent and is cooled and freshened gradually by the contact with surface and shelf waters. The modified CDW is referred to as Warm Deep Water (WDW, e.g. Carmack and Foster, 1975; Foster and Carmack, 1976). Other major water masses within the WG are: Antarctic Surface Waters (AASW), WSDW, and Weddell Sea Bottom Water (WSBW). The last two are varieties of AABW: WSDW has $-0.7\,^{\circ}\mathrm{C}<\theta<0\,^{\circ}\mathrm{C}$, and WSBW has $\theta<-0.7\,^{\circ}\mathrm{C}$. Dense water production in the Weddell Sea is predominantly a result of ocean/atmosphere and/or ocean/ice-shelf heat and freshwater exchanges. Different heat and salt exchange processes resulting from ocean/ice-shelf interactions are presumably responsible for the dense water production, which occurs over the broad southern and western continental shelves and shelf breaks (Foster and Carmack, 1976; Foldvik et al., 1985). Once formed, the dense waters flow down the adjoining continental slopes as density currents. These dense 'plumes' interleave with ambient deep water masses or form broad, sheet-like bottom layers that can be up to several hundred meters thick and in places extend over most of the continental slope (Gordon et al., 1993; Gordon, 1998). The dense sheet of bottom water flows northward along the western rim of the Weddell Sea, adjacent to the Antarctic Peninsula, and is further modified en route by additional sources along the Peninsula, such as from the Larsen Ice Shelf (Fahrbach et al., 1995; Muench and Gordon, 1995).

As these dense flows reach the northeastern tip of the Antarctic Peninsula, slope currents deeper than about 2000 m are constrained primarily by bottom topography to continue eastward along the southern flank of the South Scotia Ridge (e.g. Foster and Carmack, 1976; Orsi et al., 1993). Subject to seasonal and interannual variations, the plume splits, with part following a cyclonic path around Powell Basin and the remainder proceeding directly toward the South Orkney Plateau (Gordon et al., 2001). A shallow fraction of this flow exits into the Scotia Sea from the northern Powell Basin (Nowlin and Zenk, 1988), while a deeper fraction enters the Scotia Sea through passages in the South Scotia Ridge east of the South Orkney Islands. This deeper fraction then flows either to the Atlantic Ocean (Locarnini et al., 1993) or eastward to the abyssal plain of the Indian Ocean (Naveira Garabato et al., 2002b). The coldest components, which represent fractions of two different water types, WSDW and the less dense part of WSBW, are prevented by the bottom topography from exiting the Weddell Basin across the Ridge (Orsi et al., 1993, 1999). The South Sandwich Trench is the only route sufficiently deep to allow northward penetration of denser portions of WSBW. Nevertheless, the bottom topography and the potential vorticity balance force most of WSBW to recirculate back into the Weddell Sea (Georgi, 1981). Significant portions of modified shelf waters, near the Antarctic Peninsula, flow northward, contribute to the ventilation of the Bransfield Strait basins, and proceed to the Southwest Pacific (Gordon et al., 2000). Thus, bottom topography is a major factor in determining the pathways through which dense water, formed in the Weddell Sea, can escape into the Scotia Sea. The constraint applies throughout the water column: the weak stratification in this region implies a significant barotropic component that steers the flow along constant f/H contours, as required by potential vorticity conservation (Muench and Hellmer, 2002).

Export of AABW over the South Scotia Ridge has been recently recognized as an important outflow from the Weddell Sea (Naveira Garabato et al., 2002b). In spite of its importance, because of the scattered sampling in the region, there are few and highly variable estimates of these deep flows. Locarnini et al. (1993) estimated a northward geostrophic transport of 1.5 Sv of the AABW (relative to 1500 m) through the Orkney Passage, the deepest gap of the ridge. Short-term current measurements north of the ridge (Gordon et al., 2001) and the detection of AABW flowing over the ridge at other locations (Locarnini et al., 1993; Naveira Garabato et al., 2002a) suggest that the above estimate may not be representative of the total AABW export over the ridge. According to Naveira Garabato et al. (2002b),

the different exit routes of AABW from the Weddell Sea are related to two distinct regional forms of AABW, as reported by Carmack and Foster (1975): WSDW can flow over the ridge in regions where the dense WSBW cannot (e.g. Naveira Garabato et al., 2002a). Naveira Garabato et al. (2002b) analyzed AABW formation in the central Weddell Sea (WSDW/WSBW) and its export (as WSDW) over the South Scotia Ridge. Using Lowered Acoustic Doppler Profiler (LADCP) data they estimated a full depth geostrophic transport of 22 ± 7 Sv over the ridge and a WSDW outflow of 6.7 ± 1.7 Sv. When a box inverse model using non-synoptic hydrographic data was applied, these transports decreased to 7 ± 6 and 4.7 ± 0.7 Sv, respectively. The latter WSDW outflow is a factor of 4 larger than the 1.5 Sv estimated by Locarnini et al. (1993) and is closer to the 6.4 Sv obtained by Schodlok et al. (2002) using a numerical simulation. The inverse model diagnosed that 9.7 ± 3.7 Sv of AABW (5.8 ± 3 Sv of WSDW and 3.9 ± 0.8 Sv of WSBW) are formed in the Weddell Sea and about 48% of that flows across the ridge while the remainder flows eastward south of the ridge.

3. Data set and methods

3.1. Hydrographic data

During the austral summers of 2000 and 2001 two oceanographic cruises, referred to as ARXVIII and ARXIX, were carried out in the northwestern Weddell Sea on board the RV ARY RONGEL. Hydrographic data were collected using a Sea-Bird 911plus CTD system and an SBE 32 carrousel equipped with 12 5-L bottles. Data processing and calibration procedures are described in Schröder et al. (2002) for the ARXVIII cruise. In both cruises data accuracies were 2 mK (temperature), 2 dbar (pressure), and 0.003 (salinity) (H. Hellmer, pers. comm., 2005). During both cruises, hydrographic sections were occupied bounding the main deep gaps over the South Scotia Ridge, and the height of the CTD above the bottom was monitored using a Datasonic altimeter, providing observations to about 10 m from the sea floor. The sampling was designed to enclose portions of the northwestern Weddell Sea that allow application of box inverse models to determine the full-depth geostrophic transport through the gaps of the ridge (Fig. 1). Two boxes were constructed using the ARXVIII data. One box bounds the Philip Passage (**I**) and the southern Powell Basin (**II**), while the other box bounds the Orkney Passage (**III**), the region southwest of Bruce Passage (**IV**) and part of the northern edge of the WG (**V**). Extensive sea ice coverage during the summer of 2001 prevented the reoccupation of hydrographic stations in the southern Powell Basin and in the Orkney and Bruce Passages. Thus, only one box was constructed using ARXIX data, with sections occupied over the Philip Passage (**VI**) and the central Powell Basin (**VII**).

3.2. Inverse method and bottom triangle extrapolation

Inverse methods combine oceanographic observations with oceanic models, which are based on

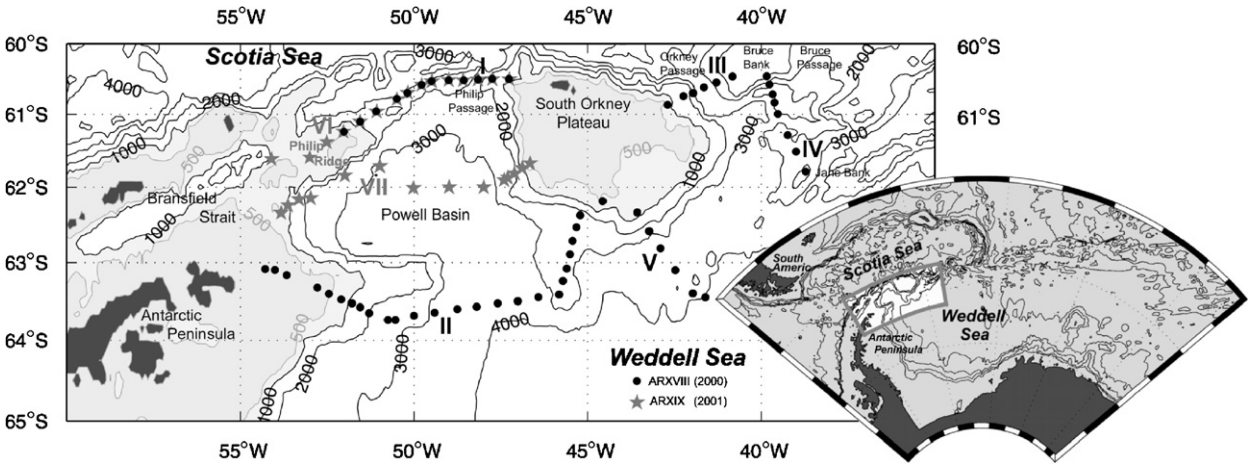

Fig. 1. Locations of the hydrographic stations occupied during the austral summers of 2000 and 2001. Stations selected to compose closed boxes for ARXVIII (●, sections **I** to **V**, 2000) and ARXIX (★, sections **VI** and **VII**, 2001) are shown. Bottom topography is from ETOPO5.

physical laws of fluid dynamics, aimed to determine factors of the ocean circulation. In the inverse theory the ocean is assumed in geostrophic and hydrostatic balance to resolve the mesoscale and large-scale circulation. The baroclinic component of the geostrophic velocity is computed through the thermal wind equation, while the barotropic component is estimated by the inverse model discretized in a set of linear equations of flow property conservation, permitting the determination of the absolute velocity (Wunsch, 1977; Roemmich, 1981). An essential factor of the inverse theory is the linearity, which allows explicit expressions to resolve inverse problems (Bennett, 1992). The box inverse theory and methods have been thoroughly discussed by Wunsch (1977, 1978, 1996). In this work, the DOBOX 4.2 software package (Morgan, 1994) was used.

The study of ocean flow in regions of sloping bottom includes uncertainties, mainly on the deep flow, which depend on the consideration or not of the bottom triangles and of the approach used to extrapolate the velocity and properties within the triangles. Some studies extrapolate property values within the bottom triangles as described by Wunsch (1996), Ganachaud (1999), and Roemmich and Wunsch (1985). The baroclinic geostrophic velocity is computed through the extrapolated data, and the baroclinic transport is calculated integrating the velocity within the triangle. We tested several extrapolation methods suggested in the literature (e.g. Roemmich and Wunsch, 1985; Wunsch, 1996; Ganachaud, 1999). However, extrapolation in several station pairs led to abrupt property gradients, unrealistic θ/S characteristics and/or density inversions. The 'constant slope' (isotherm sloping) method suggested by Ganachaud (1999) produced the most realistic results, mainly because, unlike others methods, it considers the deep gradients at shallow stations. This consideration allows extrapolation of the dense near-bottom water characteristics from the shallow station. Bottom triangle extrapolation methods can only supply an approximation of the flow between the shallow and the deep station. Property fluxes associated with narrow bottom flows between stations cannot be properly quantified. In this work, potential temperature and salinity were linearly extrapolated within the bottom triangles using the deepest 50 m of the shallow station. The procedure is based on the quasi-linear mixing line of WDW–WSDW–WSBW in θ/S space. Linear θ and S extrapolations were considered unrealistic when the resulting water mass differed from the regional θ/S distributions observed along each transect. Extrapolations were not carried out when, at a given potential temperature, extrapolated salinity differed from the observed values by >0.01. At any given θ most extrapolated salinities fell within 0.005 of the observed values. Whenever the linear θ/S extrapolations led to unrealistic water mass characteristics in θ/S values, the bottom values of the shallow station were used for extrapolation. The extrapolations were carried out up to half the depth of the bottom triangle. In addition to producing realistic water mass characteristics, in most cases the extrapolation procedure led to a nearly linear baroclinic geostrophic velocity within the bottom triangle. The baroclinic geostrophic velocity was computed relative to the sea surface. When the extrapolation procedure led to inversions of baroclinic velocity, no extrapolation was carried out.

4. Export of the deep flow in the northwestern Weddell Sea

4.1. Layer definitions

Following Naveira Garabato et al. (2002b) the boundaries between the main water masses were selected based on neutral density (γ^n) surfaces (Jackett and McDougall, 1997). The neutral density surfaces have been thoroughly used in inverse models and, according to Naveira Garabato et al. (2003), these surfaces are the most appropriate water mass boundaries for studies of ocean circulation. Neutral density values of 28.00, 28.26, and 28.40 $\mathrm{kg\,m^{-3}}$ were selected as the AASW/WDW, WDW/WSDW, and WSDW/WSBW interfaces, respectively (Table 1). The first of these γ^n values marks the boundary between the Upper and Lower CDW sublayers in Drake Passage (e.g. Naveira Garabato et al., 2002a). As the southern boundary of the ACC coincides with the poleward edge of Upper CDW sublayer (e.g. Orsi et al., 1995), this boundary is a reasonable approximation to the density of the lightest CDW injected into the eastern WG from the ACC and later transformed to WDW. The value of $\gamma^n = 28.26\,\mathrm{kg\,m^{-3}}$ separates WSDW from the ACC in the Scotia Sea (e.g. Naveira Garabato et al., 2002a) whereas in the northern Weddell Sea $\gamma^n = 28.40\,\mathrm{kg\,m^{-3}}$ coincides with the $\theta = -0.7\,^{\circ}\mathrm{C}$ isotherm, which was originally defined as the WSDW/WSBW boundary by Carmack and

Table 1
Model layer definitions and equivalence with the main water masses

Layer boundary	Upper interface γ^n (kg m^{-3})	Water mass
1	Surface	AASW
2	27.90	
3	28.00	WDW
4	28.10	
5	28.20	
6	28.26	WSDW
7	28.31	LWSDW
8	28.40	WSBW
9	Bottom	

Foster (1975). Recent studies have shown that lower WSDW (LWSDW) is too dense to overflow the Georgia Passage east of the Scotia Sea, which is another WSDW pathway out of the Weddell basin (e.g. Arhan et al., 1999; Naveira Garabato et al., 2002a). Thus, we subdivide WSDW into an Upper and Lower layer at $\gamma^n = 28.31\,\mathrm{kg\,m^{-3}}$. In addition to these four water mass boundaries, because WDW occupies most of the water column in the Philip Passage, we partitioned WDW into three layers separated by $\gamma^n = 28.10$ and $28.20\,\mathrm{kg\,m^{-3}}$. Finally, parts of AASW are in contact with the atmosphere and sea ice, inducing non-conservation of temperature and salinity; we therefore defined an additional interface ($\gamma^n = 27.90\,\mathrm{kg\,m^{-3}}$) subdividing AASW in two layers, and we excluded the uppermost layer from the property conservation equations.

4.2. Cruise ARXVIII (2000)

4.2.1. Box over the Powell Basin

4.2.1.1. Philip Passage. Section **I** over the Philip Passage (~48°W), located within the Weddell–Scotia Confluence, bounds the Powell Basin to the north. AASW is the warmest and shallowest water mass throughout the section, extending down to about 200 m (Fig. 2a and c). WDW, characterized by mid-depth potential temperature and salinity maxima, extends to approximately 1300 m. In this layer warm ($\theta > 0.4\,^\circ$C) and salty ($S > 34.67$) waters are located in the eastern part of the Philip Passage (Fig. 2a and b). WSDW forms a near-bottom layer along the sloping topography, mostly on the central part of the section (Fig. 2c). The neutral density surface $\gamma^n = 28.26\,\mathrm{kg\,m^{-3}}$, which characterizes the top of WSDW, is closer to the $\theta = -0.2\,^\circ$C isotherm than to the $\theta = 0\,^\circ$C isotherm, which suggests deep mixing generated in this region. In most station pairs the linear property extrapolation within the bottom triangles leads to realistic θ/S characteristics, except for the easternmost pair, where the constant extrapolation of the deepest observations at the shallow station is used (Fig. 3a). The extrapolations lead to an increase of up to $2\,\mathrm{cm\,s^{-1}}$ of baroclinic geostrophic velocities (Fig. 3b).

4.2.1.2. Southern Powell Basin. Section **II** runs from the tip of the Antarctic Peninsula in an east-southeast direction down the continental slope into the deep Weddell Sea, continuing to the southern entrance of the Powell Basin in a more easterly and northerly direction toward the continental slope of the South Orkney Plateau (Fig. 1). The region covered by the section resolves the water masses circulating within the Powell Basin (see Fahrbach et al., 1994, 2001; Gordon et al., 2001; von Gyldenfeldt et al., 2002). The isopleth tilt of WDW relative to the bottom indicates a dominant cyclonic circulation in the Powell Basin, with inflow along the continental slope off the Antarctic Peninsula and the return flow along the western slope of the South Orkney Plateau (Fig. 2a and b). This is in agreement with the results of Schröder et al. (2002). AASW occupies the shallowest depths ~100–200 m, and, in the two westernmost stations, it extends down to about 400 m (Fig. 2c). WDW extends along the continental slope of the peninsula and rises in the central section to approximately 1500 m. LWSDW fills most of the water column below 2000 m. The cold and fresh lens hugging the continental slope of the Antarctic Peninsula marks the newly formed WSBW (e.g. Absy, 2003; Schröder et al., 2002). WSBW flows eastward within the northern limb of the WG. The linear property extrapolation method within the bottom triangles leads to results in agreement with the typical water mass properties in most station pairs. However, because of the large property gradients observed at station pairs 1, 6, 8, 9, and 12, the deepest θ and S observations at the shallow stations were used (Fig. 3a). Because of inversions in the baroclinic velocity, no extrapolation was applied at station pair 23. The baroclinic geostrophic velocity calculated with the extrapolated data increases to 1–3 cm s^{-1}, except in the easternmost station pair, where it increases to ~7 cm s^{-1} (Fig. 3b).

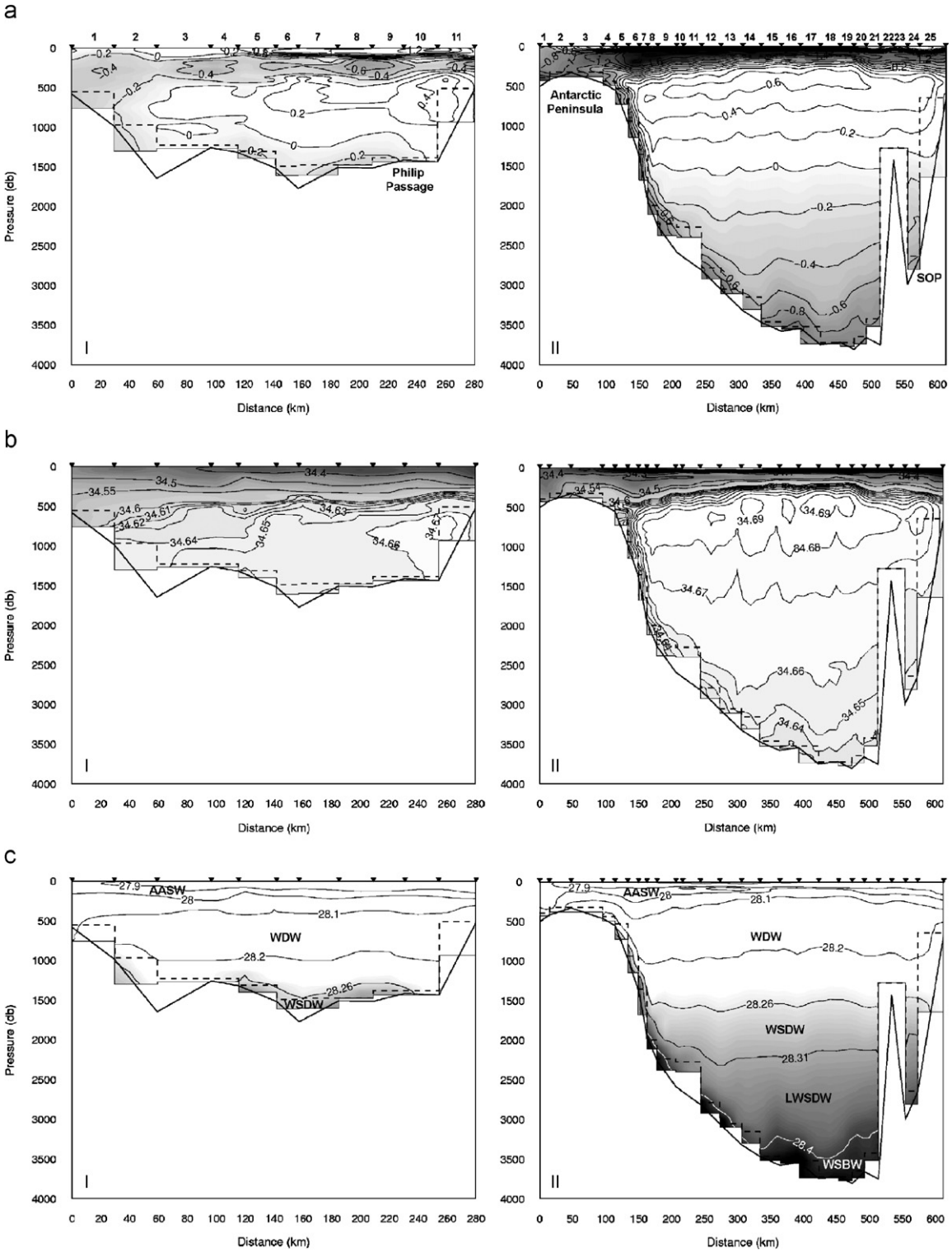

Fig. 2. (a) Potential temperature (θ), (b) salinity, and (c) neutral density γ^n (kg.m^{-3}) distributions across the Philip Passage (**I**) and southern Powell Basin (**II**) sections, occupied during the ARXVIII (2000) cruise. Water mass boundaries given by neutral density surfaces defined in Section 4.1 are shown in (c). The area added by the extrapolation within bottom triangles is indicated by the dashed line over the bottom topography (solid line). In each section station pairs are numbered in the upper panel. The location of the South Orkney Plateau (SOP) is indicated.

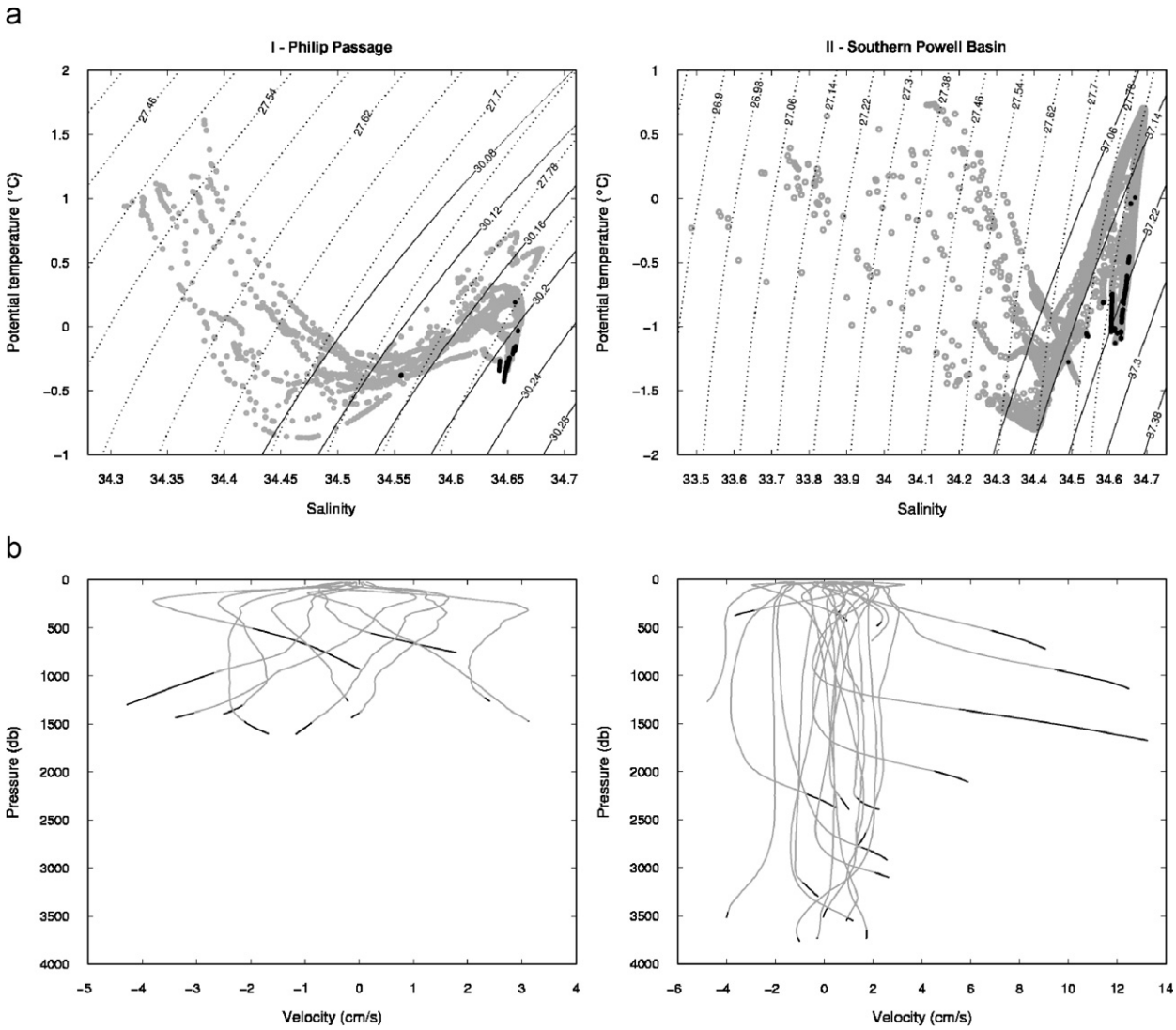

Fig. 3. (a) Potential temperature (θ)/salinity diagrams and (b) baroclinic geostrophic velocity (cm s^{-1}) for the Philip Passage (I) and southern Powell Basin (II) sections, occupied during the ARXVIII (2000) cruise. The data extrapolated to fill the bottom triangles are shown in black, overlapped by the observations (in gray). The isopycnals in the θ/S diagrams are drawn relative to the surface (σ_0, dotted line) and to 2000 m (σ_2, solid line), except in the Philip Passage, where $\sigma_{0.5}$ relative to 500 m is shown.

4.2.2. Box bounding the Orkney and southwestern Bruce Passages

4.2.2.1. Orkney Passage. Section **III** spans from the continental slope of the South Orkney Plateau to Bruce Bank, across the deepest passage of the South Scotia Ridge, the Orkney Passage, located near 42°W (Locarnini et al., 1993). This narrow passage, with depths of about 3500 m (LaBrecque et al., 1981), connects the Weddell Sea with the central Scotia Sea. AASW is the shallowest water throughout the section, extending down to about ~150–250 m (Fig. 4c). WDW occupies most of the water column down to about 1500 m on the west and 1800 m in the eastern passage. LWSDW fills the deepest part (> 2100 m) of the central passage. This layer is tilted down to about 2200 m in the west and 2450 m in the eastern passage. Relatively cold–fresh waters in the western passage cause the isopycnal tilt. According to Schröder et al. (2002) the deepest waters of the passage are occupied by WSBW derived from the northern limb of the WG. Given the sharp bottom slope in the Orkney Passage, it is expected that the bottom triangle extrapolation would strongly affect our estimates of deep-water

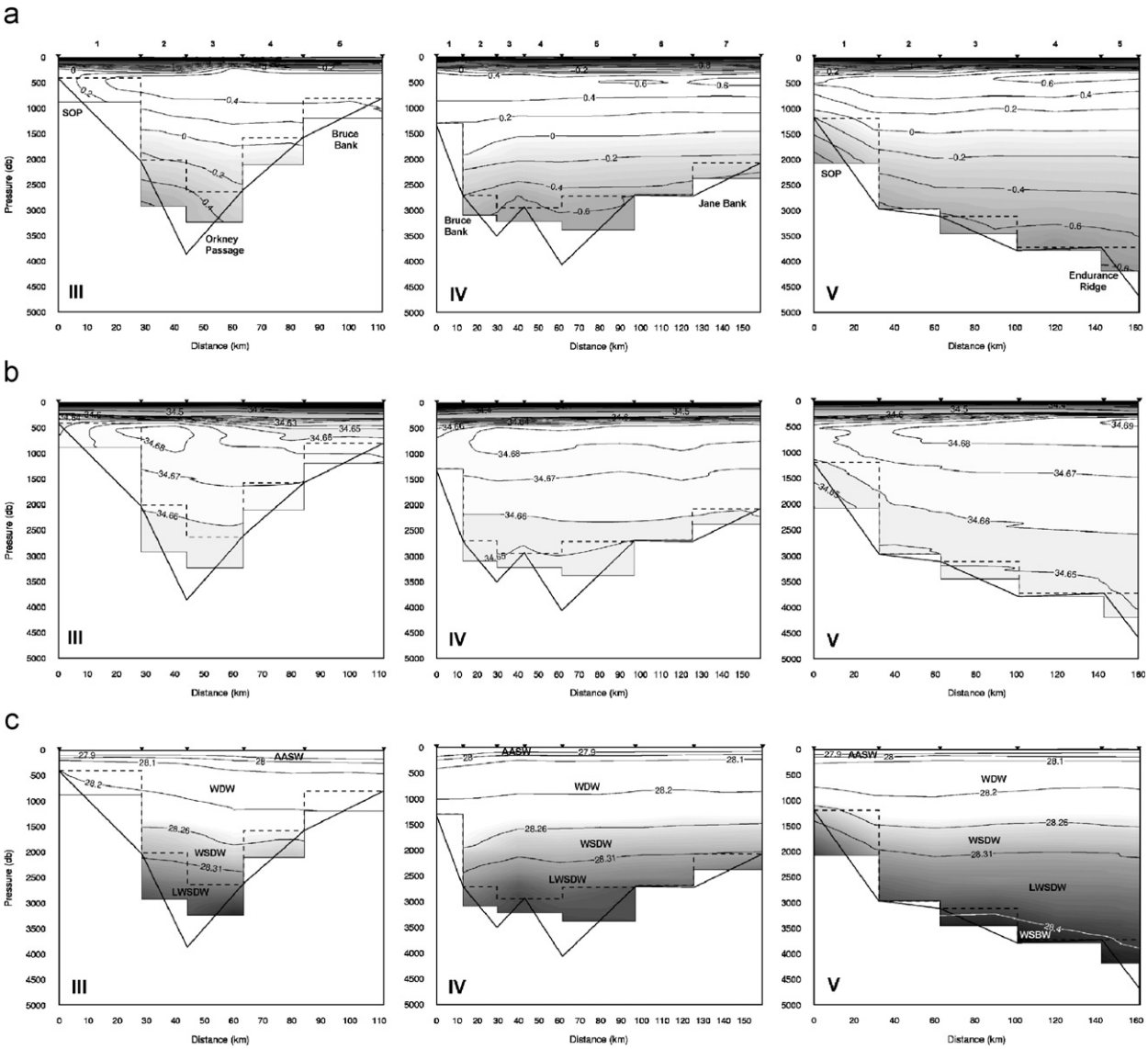

Fig. 4. (a) Potential temperature (θ), (b) salinity, and (c) neutral density γ^n (kg m^{-3}) distributions across the Orkney Passage (III), southwestern Bruce Passage (**IV**), and northern limb of the Weddell Gyre (V) sections, occupied during the ARXVIII (2000) cruise. Water mass boundaries given by neutral density surfaces defined in Section 4.1 are shown. The area added by the extrapolation within bottom triangles is indicated by the dashed line over the bottom topography (solid line). In each section station pairs are numbered in the upper panels. The location of the South Orkney Plateau (SOP) is indicated.

transport. Constant θ and S extrapolation within the bottom triangles was applied at station pairs 3 and 5. Because of the large depth difference between stations at pair 1, on which the extrapolation generates unrealistic θ/S characteristics, we chose only in this case to limit the linear extrapolation to a depth shallower than half the height of the bottom triangle. This procedure leads to a realistic θ/S distribution (Fig. 5a). The baroclinic geostrophic velocities calculated with the extrapolated data increase up to 4.5 cm s^{-1} (Fig. 5b).

4.2.2.2. Southwestern Bruce Passage. Section **IV** runs southeastward from the continental slope of Bruce Bank to the deep southwestern Bruce Passage (~38°W) and continues toward the shallow depths of Jane Bank. AASW occupies the upper layer to ~150 m, reaching 241 m in the northern station

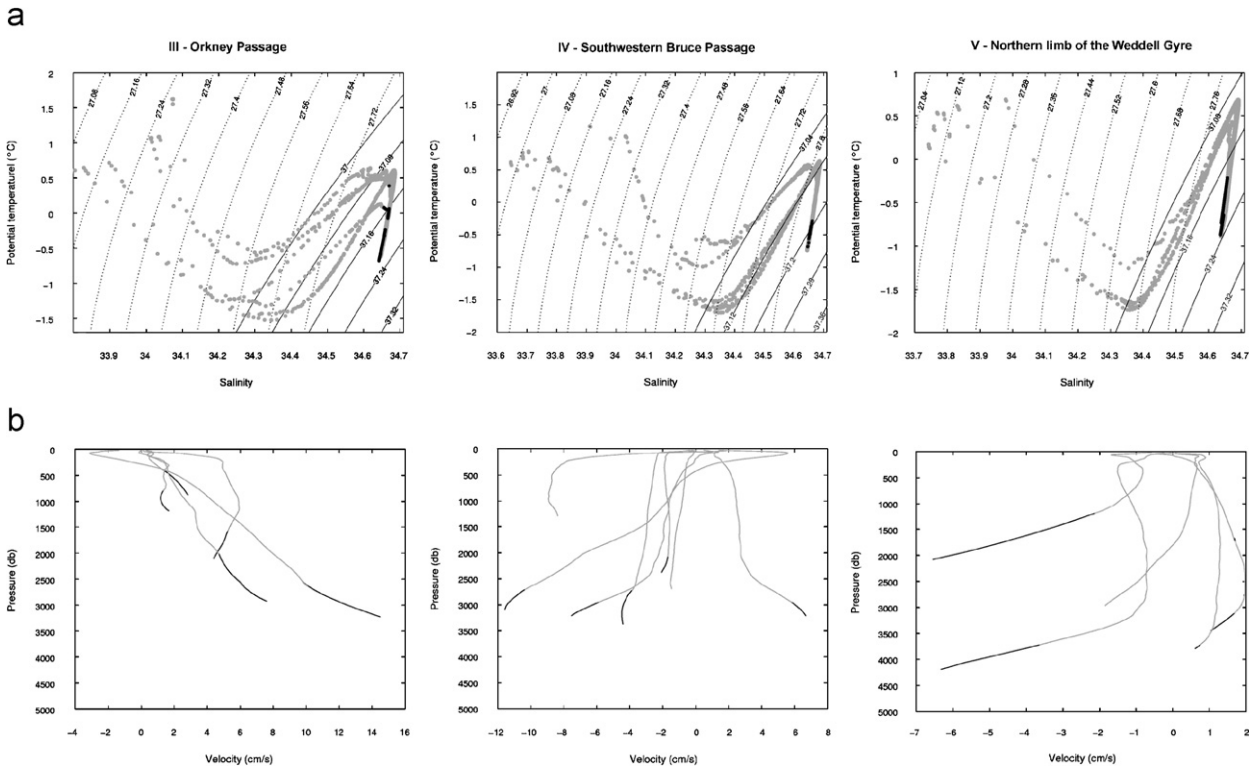

Fig. 5. (a) Potential temperature (θ)/salinity diagrams and (b) baroclinic geostrophic velocity (cm s^{-1}) for the Orkney Passage (III), southwestern Bruce Passage (IV), and northern limb of the Weddell Gyre (V) sections, occupied during the ARXVIII (2000) cruise. The data extrapolated to fill the bottom triangles are shown in black, overlapped by the observations (gray). The isopycnals in the θ/S diagrams are drawn relative to the surface (σ_0, dotted line) and to 2000 m (σ_2, solid line).

(Fig. 4c). WDW occupies a mid-depth layer to about 1600 m. At deeper levels LWSDW fills the deepest part of the passage, and WSBW is present only in the deepest station (below 3837 m). The highly linear θ/S relationship between WDW and WSDW leads to realistic results in most station pairs when linear property extrapolation is used (Fig. 5a). Constant extrapolation of near-bottom values of θ and S was applied only at station pair 5, and no extrapolation was carried out at station pair 1 because it leads to baroclinic velocity inversions. The baroclinic geostrophic velocities calculated with the extrapolated data increase up to 2 cm s^{-1} (Fig. 5b).

4.2.2.3. Northern limb of the WG. Section **V** runs southeastward from the continental slope of the South Orkney Plateau toward the deep Weddell Basin, covering part of the northern limb of the WG. Potential temperature and salinity distributions reveal a cold and fresh bottom layer on both sides of Endurance Ridge (Fig. 4a and b). According to Schröder et al. (2002), these water mass properties are characteristic of the Weddell Sea interior. The section resolves the eastward outflow from the Powell Basin and, in deeper layers, from the northwestern limb of the WG (Gordon et al., 2001; von Gyldenfeldt et al., 2002). AASW occupies the upper layer to ~140 m (Fig. 4c). Below the AASW layer, WDW is tilted along the continental slope of the plateau and rises at the center-southern section to about 1500 m. Below 2000 m most of the stations in this section present LWSDW. WSBW is observed over the bottom within the northern limb of the Weddell Gyre. The linear θ and S extrapolation within the bottom triangles was applied at all station pairs (Fig. 5a). The baroclinic geostrophic velocities calculated with the extrapolated data increase up to 4 cm s^{-1} (Fig. 5b).

4.2.3. Inverse solutions and WSDW outflow

The low stratification and reduced baroclinic shear in the northwestern WG lead to a circulation dominated largely by narrow barotropic jets (Gordon et al., 2001; Naveira Garabato et al., 2002b). Usually, in areas of weak stratification the

oceanic currents are strongly steered by the bottom topography. The western WG circulation is dominated by boundary currents that flow northward nearly parallel to the isobaths over the continental slope (Fahrbach et al., 1994). Over and near the continental slopes the flow direction is vertically coherent throughout the water column, but in the interior, where the flow is weak and variable, there are some reversals (Fahrbach et al., 1994). Instantaneous current measurements (LADCP) also suggest the largely barotropic component of velocity in the area (Gordon et al., 2001; Naveira Garabato et al., 2002b). Naveira Garabato et al. (2003) pointed out that the circulation into the WG cannot be reasonably approximated with a level of no motion because it is dominated by narrow, largely barotropic jets. In addition, other inverse analyses used direct velocity measurements and concluded they have no significant impact on the solution (e.g. Gille, 1999). In the inverse theory the barotropic velocity is well defined in the model equations until, as the solution rank increases, the noise in the solution also increases. Thus, there is a tradeoff between the number of equations used in the inversion and the stability of the solution (Roemmich, 1981). Since our boxes are not in the WG interior, to investigate the above-mentioned issues, in this work we estimated the geostrophic velocity relative to the deepest common depth at each station pair and searched for barotropic solutions that best agreed with the bottom velocity patterns described in the literature. To improve the conditioning of the inverse model, resulting in higher rank model equation matrix and hence larger barotropic solutions, in this work we attempted to reduce the noise in the solutions by considering the flow uncertainties in the set of equations.

There are several sources of noise in the inverse calculation, but the most significant are derived from internal wave activity, ageostrophic flows, and bottom triangle extrapolations (e.g. Ganachaud, 1999). Time variability in non-synoptic studies can also lead to significant flow uncertainties (Roemmich and Wunsch, 1985; Rintoul, 1991; Macdonald, 1993). During the ARXVIII cruise, the hydrographic stations that bound the Powell Basin were occupied in 15 days, from 24 January to 7 February 2000, and the Orkney and southwestern Bruce Passages and the northern WG stations were sampled in 7 days, from 30 January to 5 February 2000. We have no information on the impact of mesoscale variability in the region over these time scales; thus this possible source of uncertainty was not evaluated. However, these time scales span the spring-neap tidal interval, and interactions between strong barotropic tidal currents and bottom slopes may induce tidal conversion to internal waves in the region (see Naveira Garabato et al., 2004; Padman et al., 2006). Since we calculate the transport within the bottom triangles, in this work only the flow uncertainties induced by internal waves, tides, and Ekman ageostrophic dynamics and their impact on the solutions were estimated. The internal wave flow uncertainties were calculated using the Garrett–Munk spectrum scaled by the appropriate ratio of the Coriolis parameter (see Ganachaud, 1999; e.g. Garrett and Munk, 1979; Munk, 1981). The tidal flow uncertainties were estimated according to mean tidal velocities simulated by Padman et al. (2006). Ekman transport flow uncertainties were estimated following Naveira Garabato et al. (2002b). Station spacing larger than the internal deformation radius in the northwestern Weddell Sea, which varies between 10 and 15 km, could introduce property flux errors in our estimates. However, the rather scattered sampling in the region does not allow us to assess the possible impact of this error source on the final transport estimates.

4.2.3.1. Model configuration. To determine the geostrophic volume transports in each box, mass, salt, and heat were assumed to be conserved within layers not in direct contact with the atmosphere. The internal wave flow estimate uncertainties are ± 1.7 Sv (Section 4.2.3). Tidal flow uncertainty estimates were calculated and applied only in the boxes over the Powell Basin, since over the Orkney and Bruce Passages the tidal current velocity is expected to be weak (Padman et al., 2006). Tidal mean absolute velocities of 8 cm s^{-1} estimated in the Philip Passage (Padman et al., 2006) lead to a tidal flow uncertainty of 0.03 Sv. Ekman transport estimate uncertainties are ± 0.2 Sv based on the values of 0.5–0.6 Sv reported over a larger area of the South Scotia Ridge (e.g. Naveira Garabato et al., 2003). Each equation was normalized with the layer property mean and each column was normalized with the station pair area. The total water column equations were weighted by the flow estimate uncertainties (i.e., Ekman + internal waves and tides), and each layer below the surface layer, was weighted by the internal wave and tide uncertainty, distributed throughout the water column (± 0.22 Sv in each layer). This procedure

was applied because of the limited knowledge on the behavior of internal waves in the region, the low stratification throughout the water column, and the influence of the bottom topography, which induces conversion of strong barotropic tidal currents to internal waves (Padman et al., 2006). In the box over the Orkney and Bruce Passages, where the tides are weak, only the Ekman and internal wave flow uncertainties were considered. The first two station pairs in the Powell Basin off the Antarctic Peninsula present a nearly linear θ/S distribution, characteristic of shelf waters in this region. Recent studies have shown that these shelf waters in the western Powell Basin are steered toward the Bransfield Strait (Schodlok et al., 2002; von Gyldenfeldt et al., 2002). Since our observations do not resolve the shelf water outflow to the Bransfield Strait, we excluded these shallow waters from the mass and property flux conservation equations. In the box enclosing the Orkney Passage, southwestern Bruce Passage and the northern limb of the WG we assumed that the flow within the box is conserved. The row- and column-weighted system of equations in each box was solved by singular value decomposition (Lanczos, 1961; Wunsch, 1978, 1996).

4.2.3.2. Solutions. In each box we configured six models. The models test the combined effects of property conservation, property anomaly conservation, flow uncertainties, and bottom triangle transports. Property anomaly conservation reduces the impact of noisy mass-flux divergences on the property-flux divergences, effectively resulting in a higher rank model equation matrix (McIntosh and Rintoul, 1997; Ganachaud, 1999; Naveira Garabato et al., 2003). To formulate the conservation of potential temperature and salinity anomalies, the mean property values within each box were subtracted from the observations.

The flow estimate uncertainties and the bottom triangle extrapolation improve the stability of the solutions in the Powell Basin box (Table 2). Stable solutions in agreement with prior estimates of barotropic velocity based on property anomaly conservation were possible only when flow estimate uncertainties were considered. Property anomaly conservation equations weighted by flow estimate uncertainties led to northward transport of WSDW through the Philip Passage (section **I**). This result is not sensitive to bottom triangle extrapolation. Naveira Garabato et al. (2002b) report a WSDW transport through Philip Passage of 0.7 ± 0.4 Sv based on LADCP observations and -0.1 ± 0.3 Sv based on inverse models. In a numerical simulation Schodlok et al. (2002) found 2.2 Sv of northward WSDW transport through the Passage. The depth of the Philip Passage in the numerical model is 2050 m, and according to Naveira Garabato et al. (2002b) the deepest gap in the passage is about 1980 m and the deep gap west of the South Orkney Island is about 1600 m deep. Based on our observations the deepest gap west of the Island is less than 1800 m. This suggests that the northward transport of deep water may have been overestimated in the numerical model. We chose inverse solutions that lead to northward flow of the western boundary current over the continental shelf and slope of the Antarctic Peninsula and the cyclonic circulation in the Powell Basin.

Annual mean near-bottom currents in the northwestern gyre, near the tip of the Antarctic Peninsula (~64°S) and across the continental slope are about: 8 cm s^{-1} (500–1000 m), 2 cm s^{-1} (2000–3000 m), 4 cm s^{-1} (3000–4000 m) and approximately 1 cm s^{-1}

Table 2
Weddell Sea Deep Water (WSDW) transport through the Philip Passage (section **I**, ARXVIII—2000) in each model: equations of the model equation matrix (m), interval of stable solutions until the rank of the model equation matrix (k) and absolute transport (1 Sv = 10^6 m^3 s^{-1}, >0 is northward)

Model	Property	Bottom triangle	Flow uncertainties (internal waves + Ekman)	M	(k)	Philip P. WSDW (Sv)
I	Mass, salt and heat	–	–	25	5–8	-0.04 ± 0.01
II	Mass, salt and heat	Filled	–	25	10–13	0.08 ± 0.02
III	Mass, salt, and heat	–	Layers and total water column	24	5–8	-0.02 ± 0.03
IV	Mass, salt, and heat	Filled	Layers and total water column	24	8–15	0.10 ± 0.08
V	Mass and salt and heat anomalies	–	Layers and total water column	24	5–9	0.01 ± 0.01
VI	Mass and salt and heat anomalies	Filled	Layers and total water column	24	8–15	0.12 ± 0.03

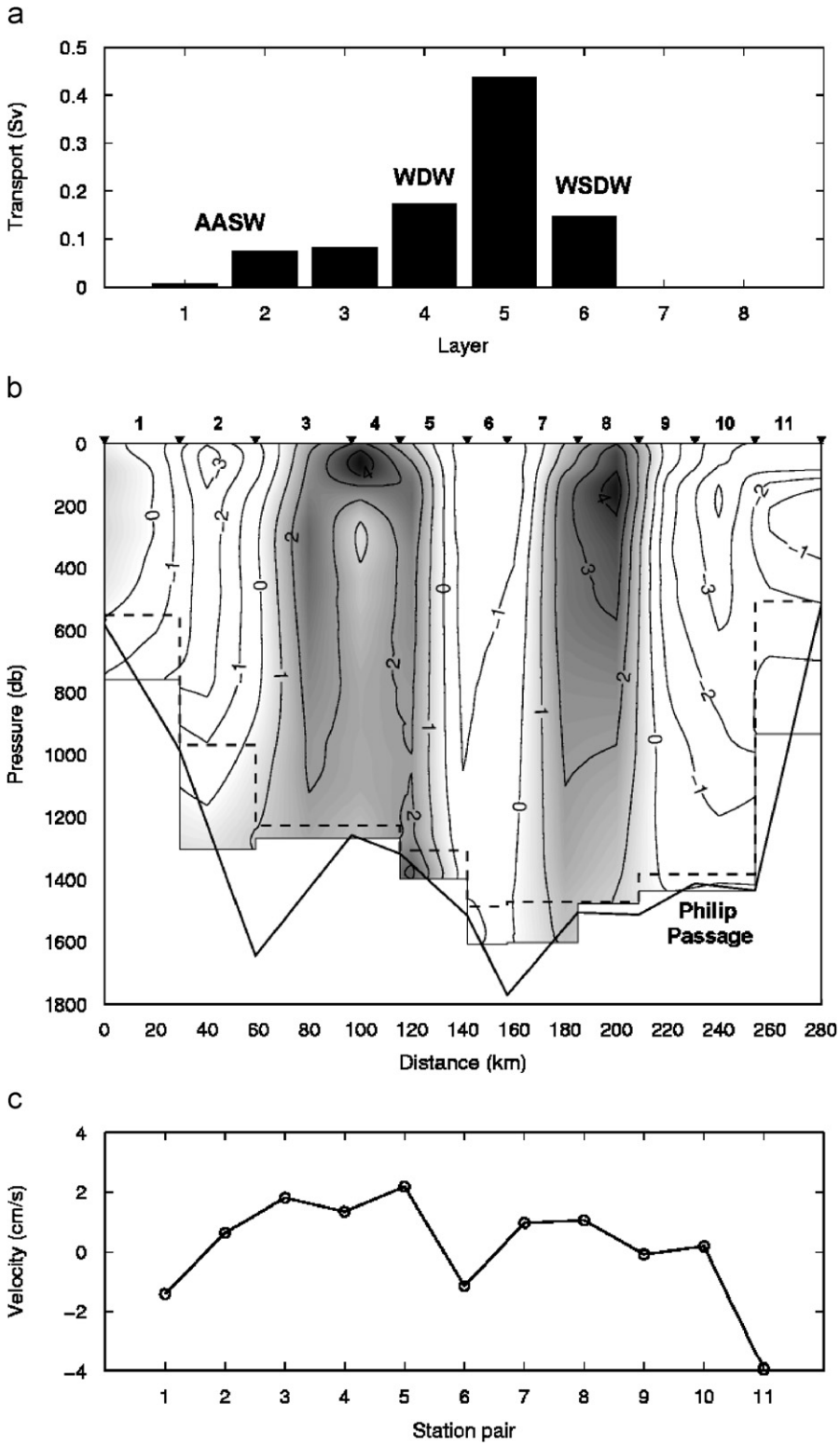

Fig. 6. (a) Layer transports through the Philip Passage (section **I**, ARXVIII 2000, $1\,\mathrm{Sv} = 10^6\,\mathrm{m}^3\,\mathrm{s}^{-1}$, >0 is northward) calculated using the rank solution ($k = 15$) of model VI. (b) Absolute and (c) barotropic velocities ($\mathrm{cm\,s}^{-1}$) across the same section. Both velocities were obtained from the rank solution ($k = 15$) of model VI; positive values are northward. The area added by the extrapolation within bottom triangles is indicated in (b) by the dashed line over the bottom topography (solid line).

below 4000 m (Fahrbach et al., 1994). Compared with these observations, the best solutions are found in model VI (Table 2), which presents similar barotropic velocities. Our solution shows a narrow countercurrent over the continental slope of the Antarctic Peninsula flowing at about 500 m with a barotropic velocity of $\sim 2\,\mathrm{cm\,s^{-1}}$. A similar southward current flowing along uniform potential vorticity contours at 400–600 m is observed in a numerical simulation (Matano et al., 2002). The easternmost flow of warm ($\theta > 0.4\,^{\circ}\mathrm{C}$) and salty ($S > 34.67$) WDW through the Philip Passage is southward, entering the Powell Basin (Fig. 6b). This is in agreement with LADCP observations (Naveira Garabato et al., 2002b). According to Matano et al. (2002), less than 1 Sv from the Scotia Sea enter through the eastern Powell Basin. Other studies suggest that a net outflow from the Powell Basin enters the Scotia Sea through the Philip Passage (Nowlin and Zenk, 1988; von Gyldenfeldt et al., 2002). Our model VI leads to 0.12 ± 0.03 Sv of WSDW and 0.84 ± 0.11 Sv of full-depth northward flow through the Philip Passage.

In the Orkney (section **III**) and southwestern Bruce (section **IV**) Passages, box inverse solutions consistent with prior results were found only when using the bottom triangle extrapolation and property anomaly equations weighted by the flow estimate uncertainty were used (Table 3). Reported WSDW transports through Orkney Passage are 4.3 ± 0.6 Sv, based on LADCP observations and 5.6 ± 0.1 Sv, based on inverse models (e.g. Naveira Garabato et al., 2002b). These results are in close agreement with the simulation of Schodlok et al. (2002), which produces 4.2 Sv of WSDW northward flow through the passage. Studies have suggested that the coldest variety of WSDW found in the Scotia Sea enters through the Orkney Passage (Wüst, 1933; Locarnini et al., 1993). Thus, the Orkney Passage is suggested as the main route of deep waters from the Weddell Sea into the Scotia Sea. The LADCP and inversion-based WSDW transport estimates through the Bruce Passage are 1.4 ± 1.2 and -0.7 ± 0.3 Sv, respectively (Naveira Garabato et al., 2002b), while the numerical simulation indicates inflows and outflow of around 0.1 Sv, with no net northward transport through the gap (Schodlok et al., 2002). The Bruce Passage is deep enough to allow export of WSDW, but little is known about the circulation in this region. The geostrophic flow of AABW exported from the Weddell Sea through the Orkney Passage, relative to 1500 m, reported by Locarnini et al. (1993) is 1.5 Sv. The bottom triangle extrapolation increases the southward WSDW transport relative to the bottom from 0.32 to 1.84 Sv. The dominant barotropic patterns considered for the choice of the inverse solutions of this box were the high northward velocities through the Orkney Passage and eastward velocities through the northern limb of the WG (not shown). Since little is known about the dominant circulation through the Bruce Passage we chose solutions of model VI, which present barotropic velocities close to the near-bottom velocities recorded by Gordon et al. (2001) in the northern limb of the WG. WSDW and full-depth outflow through the Orkney Passage obtained in model VI are 3.48 ± 1.81 and 5.81 ± 3.58 Sv, respectively. Northward barotropic velocities ($\sim 16\,\mathrm{cm\,s^{-1}}$) are higher over the west flank of the Passage than southward velocities ($< 1\,\mathrm{cm\,s^{-1}}$) over the east flank (Fig. 7c). A strong northward flow over the west flank of the Passage and a weak southward flow over the east flank are also reported by Naveira Garabato et al. (2002b) based on LADCP data and the numerical simulation of Schodlok et al. (2002). At the rank solution and the last solutions chosen, the full-depth northward outflow through the Orkney Passage is about 9 Sv, while less than 1 Sv enters into the box through the southwestern Bruce Passage (see Fig. 8)

Table 3
Weddell Sea Deep Water (WSDW) transport through the Orkney (section **III**) and southwestern Bruce (section **IV**, ARXVIII—2000) Passages in each model: equations of the model equation matrix (m), interval of stable solutions until the rank of the model equation matrix (k) and absolute transport ($1\,\mathrm{Sv} = 10^6\,\mathrm{m^3\,s^{-1}}$, >0 is northward)

Model	Property	Bottom triangle	Flow uncertainties (internal waves + Ekman)	m	(k)	Orkney P. WSDW (Sv)	Bruce P. WSDW (Sv)
I	Mass, salt and heat	–	–	25	14–16	1.79 ± 1.55	-1.41 ± 0.78
II	Mass, salt and heat	Filled	–	25	10–14	1.98 ± 0.45	1.38 ± 0.61
III	Mass, salt and heat	–	Layers and total water column	24	13–15	1.79 ± 1.24	-1.44 ± 1.25
IV	Mass, salt and heat	Filled	Layers and total water column	24	10–14	2.58 ± 0.76	0.91 ± 1.16
V	Mass and salt and heat anomalies	–	Layers and total water column	24	15–16	1.15 ± 0.33	1.03 ± 0.23
VI	Mass and salt and heat anomalies	Filled	Layers and total water column	24	12–15	3.48 ± 1.81	1.20 ± 2.16

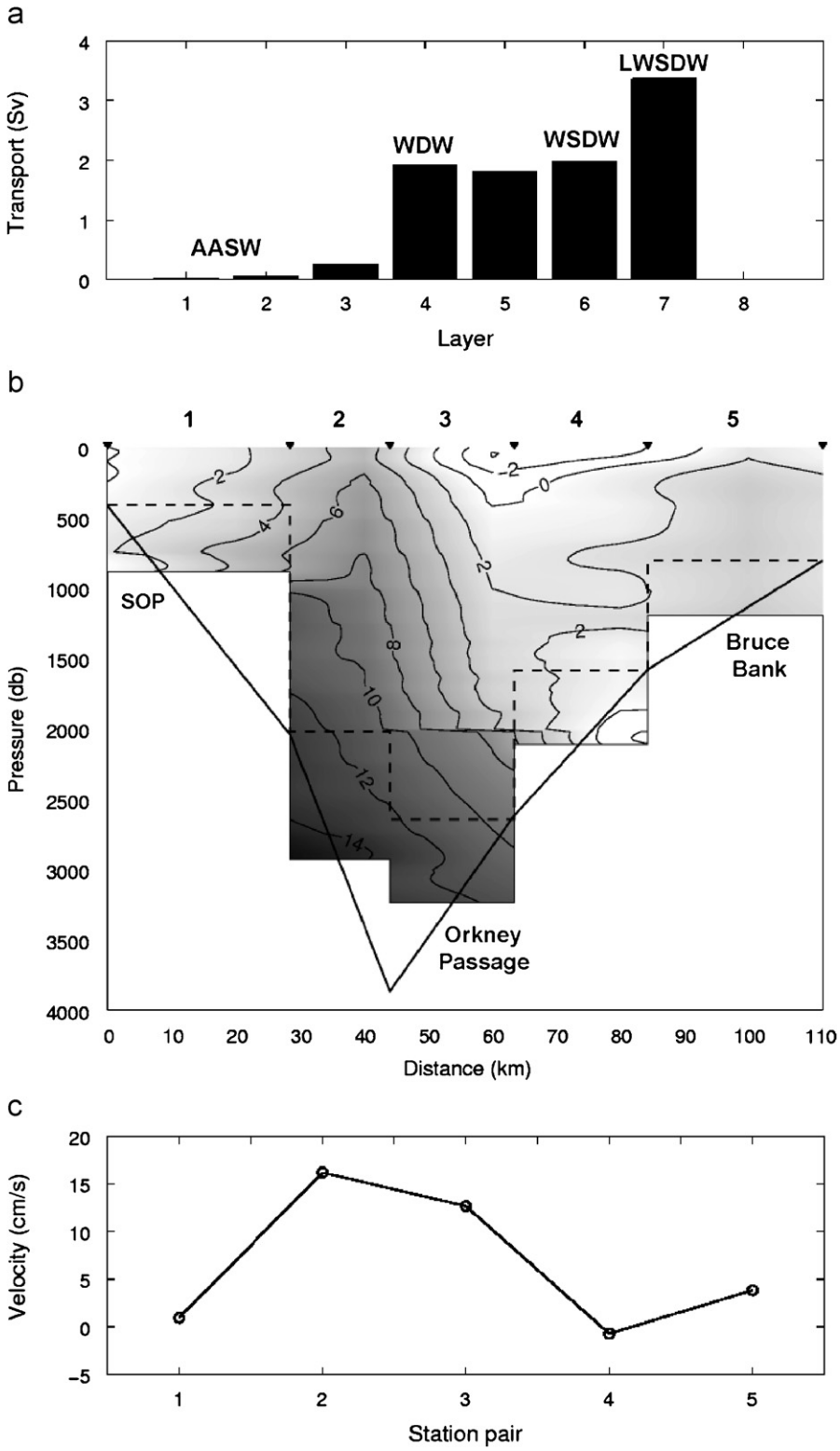

Fig. 7. (a) Layer transports through the Orkney Passage (section **III**, ARXVIII 2000, 1 Sv = $10^6\,m^3\,s^{-1}$, >0 is northward) calculated using the rank solution ($k = 15$) of model VI. (b) Absolute and (c) barotropic velocities ($cm\,s^{-1}$) across the same section. Both velocities were obtained from the rank solution ($k = 15$) of model VI; positive values are northward. The area added by the extrapolation within bottom triangles is indicated in (b) by the dashed line over the bottom topography (solid line).

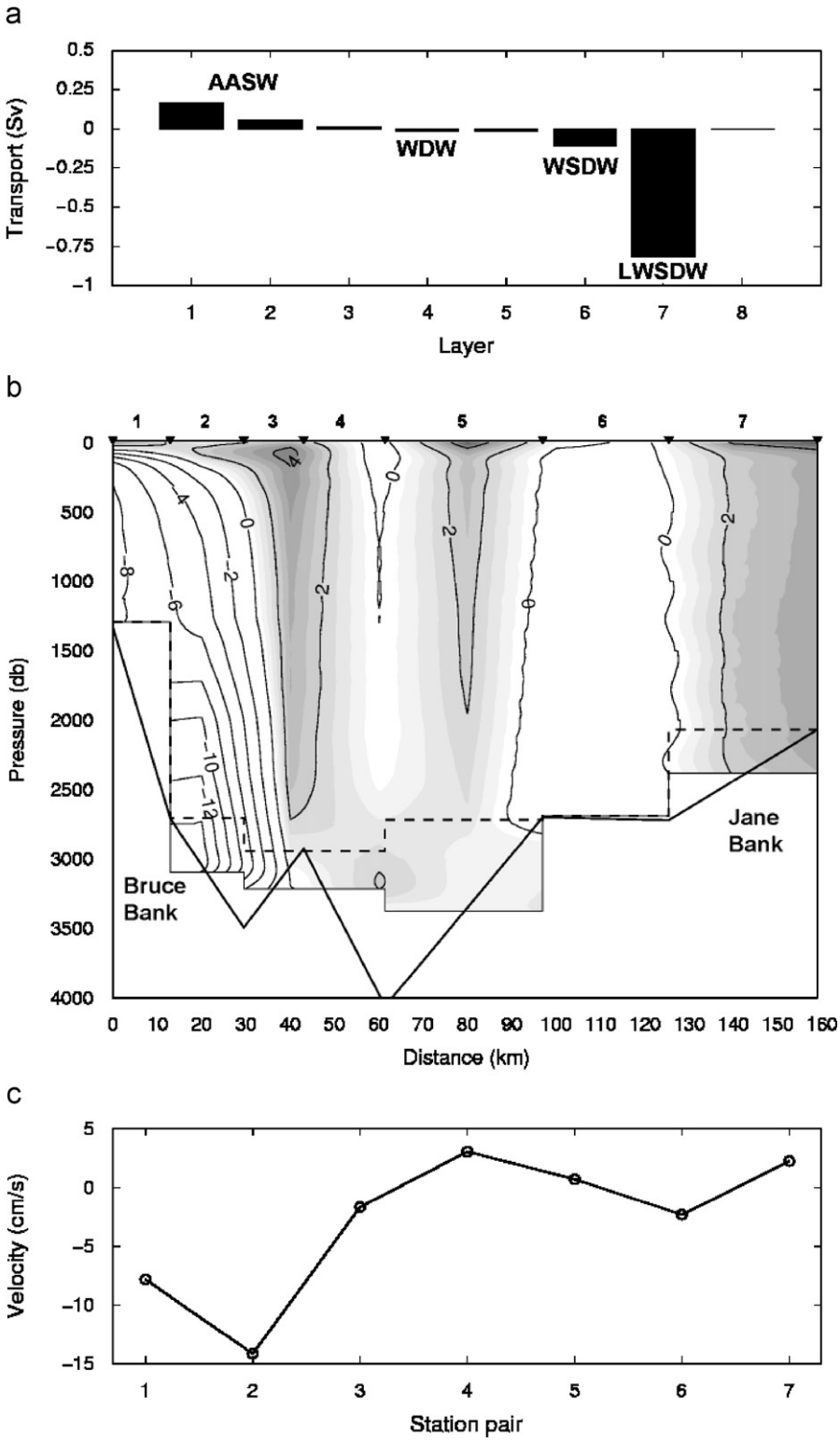

Fig. 8. (a) Layer transports through the southwestern Bruce Passage (section **IV**, ARXVIII 2000, $1\,\mathrm{Sv} = 10^6\,\mathrm{m^3\,s^{-1}}$, >0 is northward) calculated using the rank solution ($k = 15$) of model VI. (a) Absolute and (c) barotropic velocities ($\mathrm{cm\,s^{-1}}$) across the same section. Both velocities were obtained from the rank solution ($k = 15$) of model VI; positive values are northward. The area added by the extrapolation within bottom triangles is indicated in (b) by the dashed line over the bottom topography (solid line).

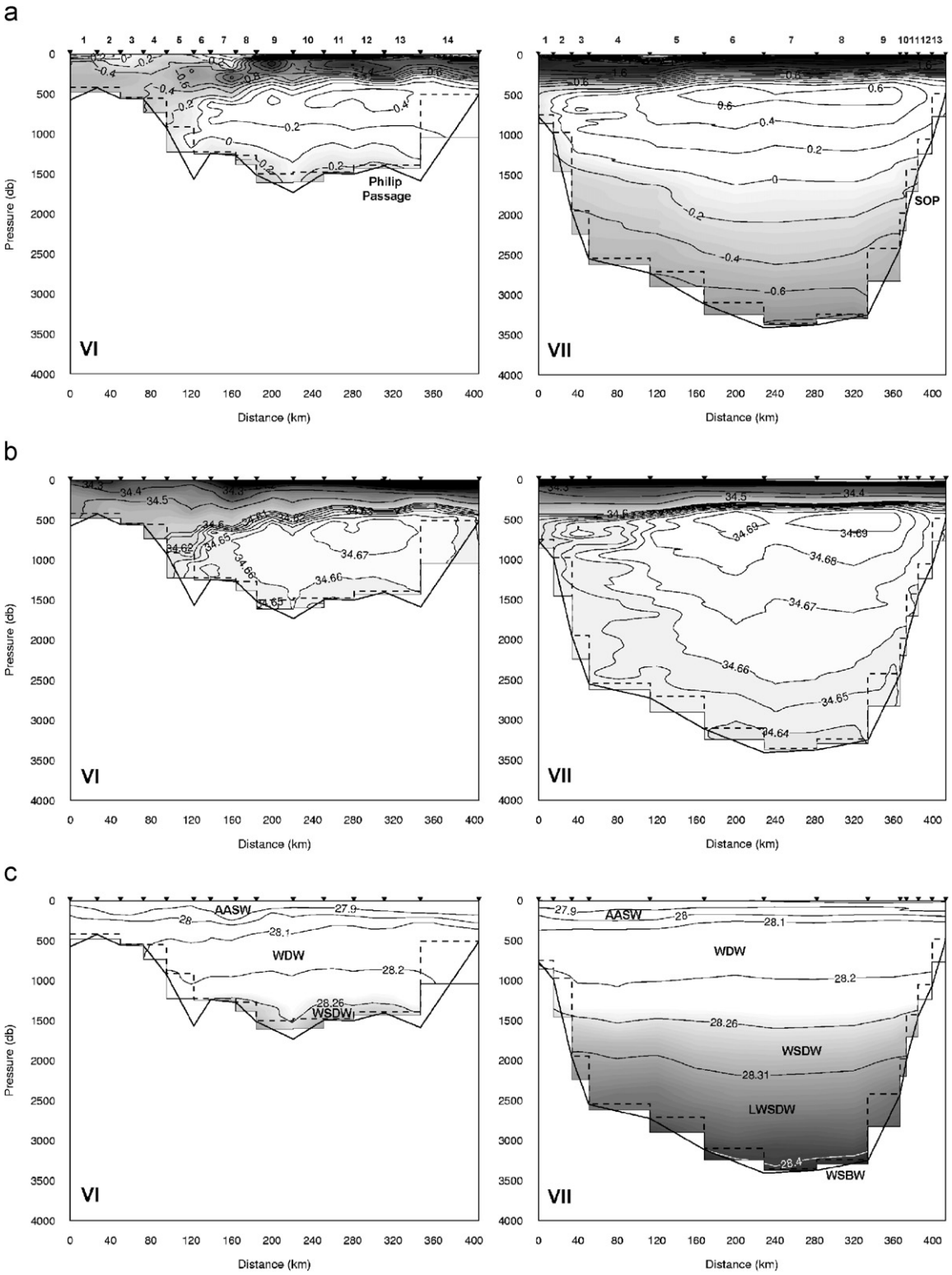

Fig. 9. (a) Potential temperature (θ), (b) salinity, and (c) neutral density γ^n (kg m^{-3}) distributions across the Philip Passage (VI) and Powell Basin (VII) sections, occupied during the ARXIX (2001) cruise. Water mass boundaries given by neutral density surfaces defined in Section 4.1 are shown. The area added by the extrapolation within bottom triangles is indicated by the dashed line over the bottom topography (solid line). In each section station pairs are numbered in the upper panel. The location of the South Orkney Plateau (SOP) is indicated.

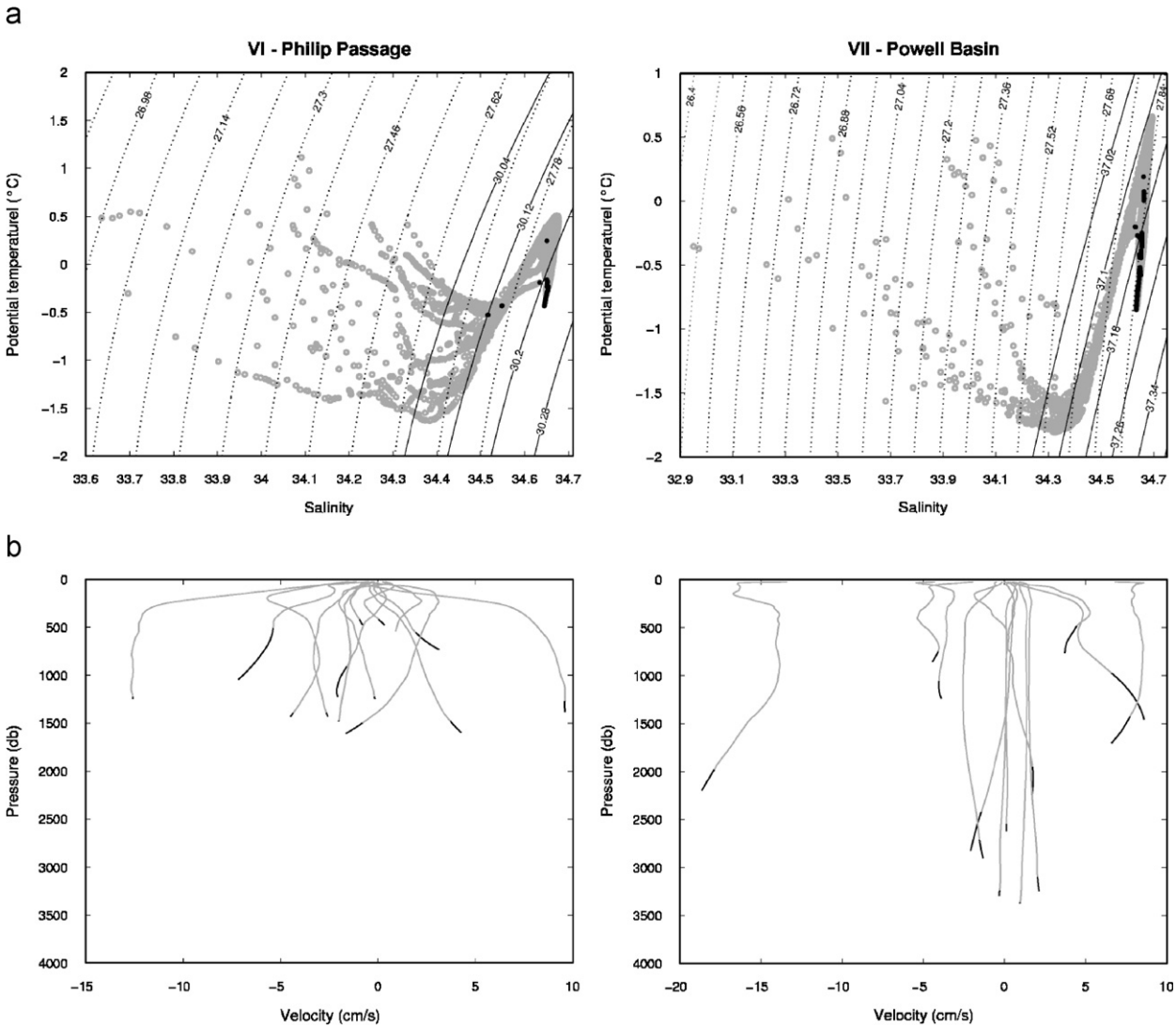

Fig. 10. (a) Potential temperature (θ)/salinity diagrams and (b) baroclinic geostrophic velocity (cm s^{-1}) for the Philip Passage (VI) and Powell Basin (VII) sections, occupied during the ARXIX (2001) cruise. The data extrapolated to fill the bottom triangles are shown in black, overlapped by the observations (in gray). The isopycnals in the θ/S diagrams are drawn relative to the surface (σ_0, dotted line) and to 2000 m (σ_2, solid line), except in the Philip Passage, where $\sigma_{0.5}$ relative to 500 m is shown.

and about 8.5 Sv flow eastward through the northern limb of the WG (not shown). In model VI the full-depth flow through the northern limb of the WG is 9.25 ± 1.01 Sv. These results are in close agreement with the numerical simulations of Matano et al. (2002). They report a full-depth northward flow of 9 Sv over the Orkney and southwestern Bruce Passages, while 22 Sv flow eastward over a larger area between the South Orkney Plateau and 65°S, crossing the northern limb of the WG at 45°W. The limited knowledge about the dominant circulation through the southwestern Bruce Passage prevents us from applying constrains to the range of solutions in this region, leading to higher flow variances.

4.3. Cruise ARXIX (2001)

4.3.1. Box over the Powell Basin

4.3.1.1. Philip Passage. Section **VI** over the Philip Passage reoccupied the positions of the hydrographic stations sampled during the ARXVIII (2000), with three additional stations taken toward the Bransfield Strait in the western end of the section (Fig. 1). AASW is the shallowest water mass

throughout the section down to about 200 m (Fig. 9c). In this layer colder ($\theta < 1.4\,^{\circ}$C) waters than found in the previous summer are located in the central-eastern part of the Philip Passage (Fig. 9a). WDW extends down to about 1300 m, with warm ($\theta > 0.4$ C) and salty ($S > 34.67$) waters located in the central-eastern part of the passage and occupying a larger area throughout the water column compared to the previous summer (Fig. 9a and b). Furthermore, warmer ($0.2\,^{\circ}\mathrm{C} < \theta < 0.4\,^{\circ}\mathrm{C}$) and saltier ($34.66 < S < 34.67$) waters also occupied a larger area in the summer of 2001. As in the previous summer, WSDW is observed in deeper layers along the sloping topography, mostly on the central gap of the section, and the neutral density surface $\gamma^{n} = 28.26\,\mathrm{kg\,m^{-3}}$ is closer to the $\theta = -0.2\,^{\circ}$C isotherm than to the $\theta = 0\,^{\circ}$C isotherm. In most station pairs the linear property extrapolation within the bottom triangles leads to realistic θ/S results, except on station pairs 1 and 10, where a constant extrapolation of the deepest observations at the shallow stations are used (Fig. 10a). The extrapolations lead to an increase of up to $2\,\mathrm{cm\,s^{-1}}$ in baroclinic geostrophic velocities (Fig. 10b).

4.3.1.2. Powell Basin. Section **VII** runs northeastward from the continental slope off the northern tip of the Antarctic Peninsula into the deep Powell Basin, and then follows a more easterly and northerly direction over the continental slope of the South Orkney Plateau (Fig. 1). AASW is observed occupying the shallowest depths ~200 m (Fig. 9c). WDW extends along the continental slopes around the basin and deepens in the central section to about 1500 m. LWSDW fills most of the deep layers. WSBW fills the bottom of the central Powell Basin down from about 3200 m. The baroclinic shear in the basin seems to be dominated by the deepest density gradients hugging the bottom topography, which would promote an anticyclonic circulation. The linear property extrapolation method within the bottom triangles leads to realistic θ/S distributions in most station pairs, except the easternmost pair, where a constant extrapolation of the deepest observations at the shallow station is applied (Fig. 10a). The baroclinic geostrophic velocities calculated with the extrapolated data increase up to $2\,\mathrm{cm\,s^{-1}}$ (Fig. 10b).

4.3.2. Inverse solutions and WSDW outflow

During the ARXIX cruise the hydrographic stations that bound the Powell Basin box were carried out in 7 days, from 22 to 28 January 2001. Thus, in this box the flow estimate uncertainties discussed and determined in Section 4.2.3 were applied.

4.3.2.1. Model configuration. Each equation and column was weighted as described in Section 4.2.3.1. Recent studies suggest intense mixing in the western Philip Ridge region, associated with waters derived from the Bransfield Strait (see von Gyldenfeldt et al., 2002). Given the flow uncertainty in this region, a relative weight 0.5 is assigned for the three westernmost station pairs in section **VI**.

4.3.2.2. Solutions. As observed in the Powell Basin inversions in 2000, the flow estimate uncertainties and the bottom triangle extrapolations improve the stability of the 2001 solutions (Table 4). The dominant barotropic pattern considered for the choice of the inverse solutions was a cyclonic circulation in the Powell Basin. The best solutions are found in model VI. Baroclinic shears

Table 4
Weddell Sea Deep Water (WSDW) transport through the Philip Passage (section **VI**, ARXIX—2001) in each model: equations of the model equation matrix (**m**), interval of stable solutions until the rank of the model equation matrix (k) and absolute transport ($1\,\mathrm{Sv} = 10^{6}\,\mathrm{m^{3}\,s^{-1}}$, >0 is northward)

Model	Property	Bottom Triangle	Flow uncertainties (internal waves + Ekman)	m	(k)	Philip P. WSDW (Sv)
I	Mass, salt and heat	–	–	25	5–10	0.03 ± 0.01
II	Mass, salt and heat	Filled	–	25	11–12	0.06 ± 0.02
III	Mass, salt and heat	–	Layers and total water column	24	5–10	0.03 ± 0.01
IV	Mass, salt and heat	Filled	Layers and total water column	24	8–11	0.07 ± 0.01
V	Mass and salt and heat anomalies	–	Layers and total water column	24	8–15	0.012 ± 0.001
VI	Mass and salt and heat anomalies	Filled	Layers andtotal water column	24	8–12	0.113 ± 0.001

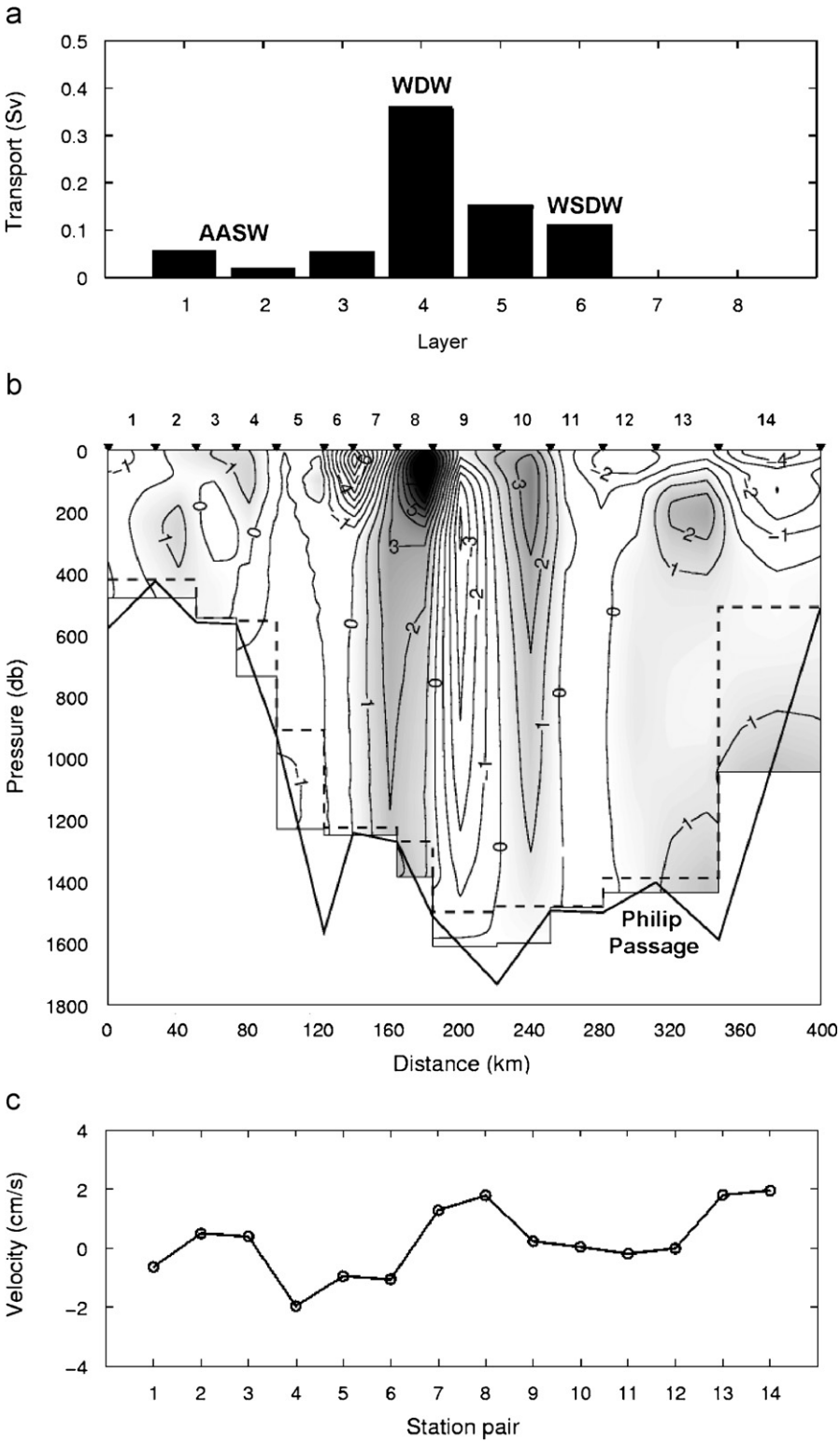

Fig. 11. (a) Layer transports through the Philip Passage (section **VI**, ARXIX 2001, $1\,\mathrm{Sv} = 10^6\,\mathrm{m}^3\,\mathrm{s}^{-1}$, >0 is northward) calculated using the rank solution ($k = 12$) of model VI. (b) Absolute and (c) barotropic velocities ($\mathrm{cm\,s}^{-1}$) across the same section. Both velocities were obtained from the rank solution ($k = 12$) of model VI; positive values are northward. The area added by the extrapolation within bottom triangles is indicated in the middle panel by the dashed line over the bottom topography (solid line).

reveal a strong meandering over the Philip Passage (section **VI**), with absolute velocities reaching about 8–10 cm s^{-1} at station pairs 7 and 8 (Fig. 11b). WSDW and full-depth outflow through the Philip Passage obtained in model VI are 0.113 ± 0.001 and 0.72 ± 0.06 Sv, respectively. Therefore, WSDW outflow in the summer of 2001 is similar to the 0.12 ± 0.03 Sv estimated in the summer of 2000. In contrast, the circulation derived from the inversion in the summer of 2001 suggests a sharp weakening of the barotropic cyclonic flow in the Powell Basin. Barotropic velocities lower than 1 cm s^{-1} occupy most of the section over the basin and increase to 4 cm s^{-1} in the westernmost station pair, which results in a dominant anticyclonic baroclinic pattern throughout the Powell Basin (not shown).

5. Hydrographic and Environmental Differences During the Austral Summers of 2000 and 2001

5.1. Hydrographic differences

Significant differences in the hydrographic properties of WDW and in mesoscale features observed west of South Orkney Island are apparent when the data gathered during the ARXVIII (2000) and

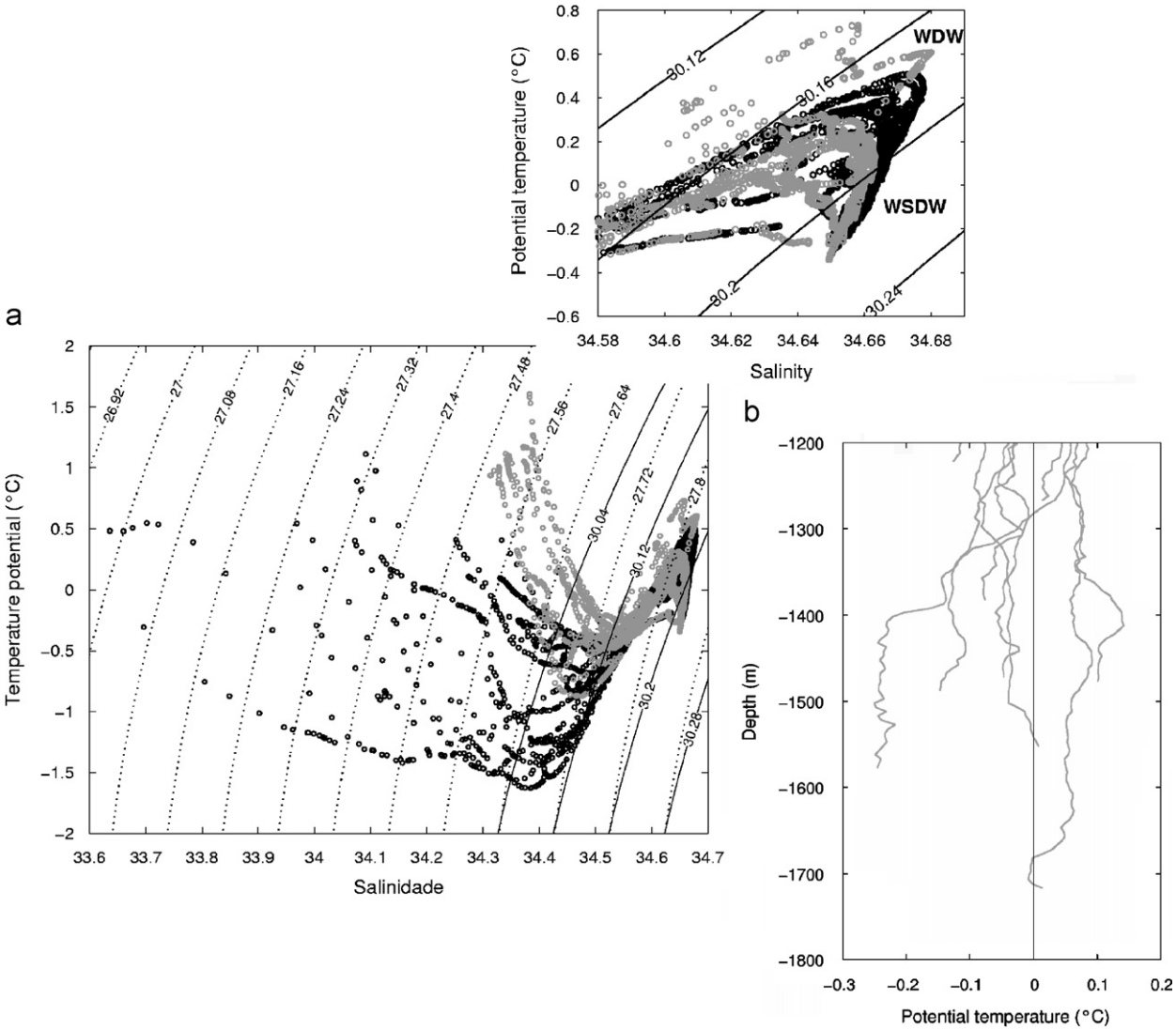

Fig. 12. (a) Potential temperature (θ)/salinity diagram for the hydrographic stations over the Philip Passage during ARXVIII—2000 (gray) and ARXIX—2001 (black). The isopycnals are drawn relative to the surface (σ_0, dotted line) and to 500 m ($\sigma_{0.5}$, solid line). The inset shows the detailed WDW θ/S characteristics. (b) Potential temperature difference (2001–2000, in °C) at the stations occupied in both years.

ARXIX (2001) cruises are compared. Von Gyldenfeldt et al. (2002) suggested that the complex topography to the north of Powell Basin can induce meandering and eddies. Several studies have documented hydrographic variations of WDW properties in the Weddell Sea (see Meredith et al., 2001; Robertson et al., 2002; Schröder et al., 2002; Fahrbach et al., 2004). Von Gyldenfeldt et al. (2002) pointed out a recent WDW warming trend over the Philip Passage in the northern Powell Basin. Colder and fresher surface waters are observed across the hydrographic section over the Philip Passage taken during the summer of 2001 than in 2000 (Fig. 12a). Warmer and saltier WDW and colder WSDW were also observed in 2001 than in 2000 (Fig. 12a and b). The WDW potential temperature maximum is approximately 0.2 °C higher and approximately 0.02 saltier in 2001 than in the previous summer. WSDW below about 1300 m was up to 0.25 °C colder in the summer of 2001 (Fig. 12b). The warmest WDW ($\theta \sim 0.73$ °C) observed in the Philip Passage in 2000 was in the eastern passage (Fig. 2a). According to the circulation derived from the inversion these waters flow southward through the Philip Passage, which suggests mixing with warmer waters from the Scotia Sea (see Fig. 9b).

5.2. Atmospheric conditions

Sea-level pressure (SLP) and sea-surface wind stress data from the National Center for Environmental Prediction/National Center for Atmospheric Research (NCEP/NCAR) Reanalysis Project (Kalnay et al., 1996) were used to characterize the large-scale atmospheric conditions in summer (December–February) of 2000 and 2001. SLP data are supplied by NOAA-CIRES Climate Diagnostics Center (http://www.cdc.noaa.gov) over a $2.5° \times 2.5°$ grid. Monthly mean sea-surface wind stress data are provided by NOAA-CDAS1 and obtained through the International Research Institute for Climate and Society (IRI/LDEO Climate Data Library, http://ingrid.ldeo.columbia.edu). During the summer of 2000 a low SLP center (<981 hPa) located east of the Antarctic Peninsula induced northwesterly winds over the northwestern Weddell Sea and the Powell Basin (Fig. 13). In contrast, during the following summer, northerly and northeasterly winds, associated with a low-pressure center located west of the Peninsula, are observed. Anomalous atmospheric patterns periodically reaching the Weddell Sea from the west are known to perturb the sea ice circulation and distribution (Venegas and Drinkwater, 2001). Since the oceanic flow is largely

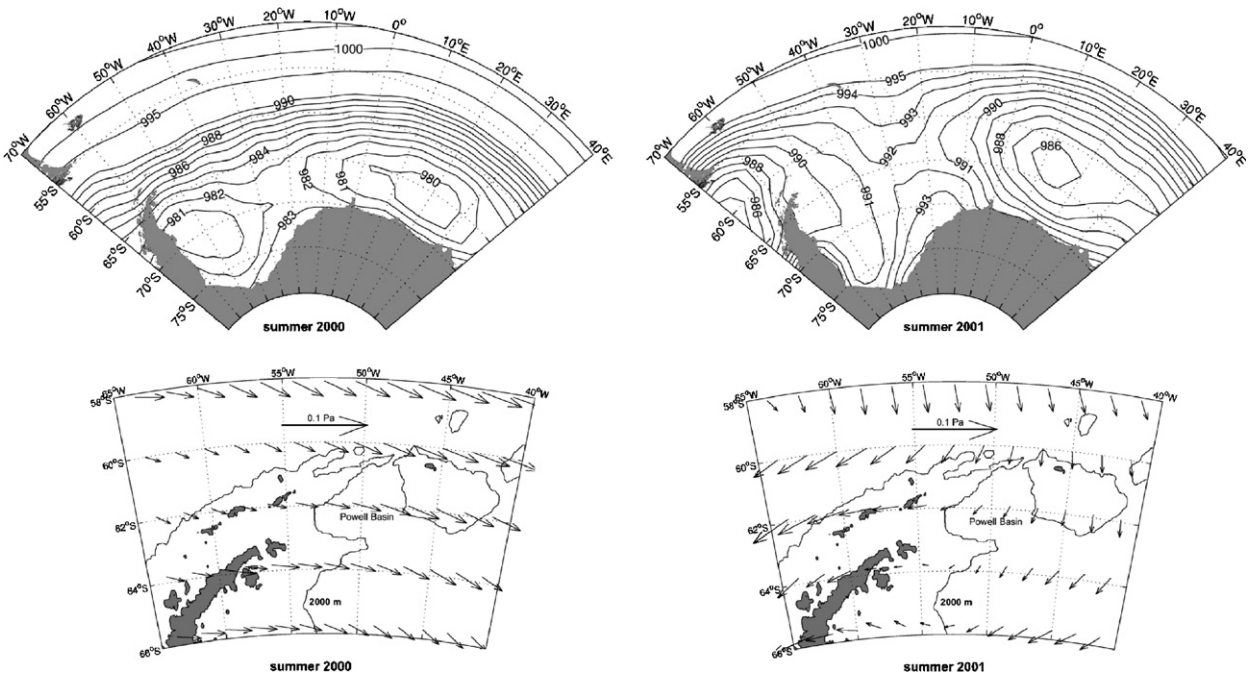

Fig. 13. Sea-level pressure (hPa, upper panels) and sea-surface wind stress vectors (Pa, lower panels) during the austral summers (December–February) of 2000 (left) and 2001 (right).

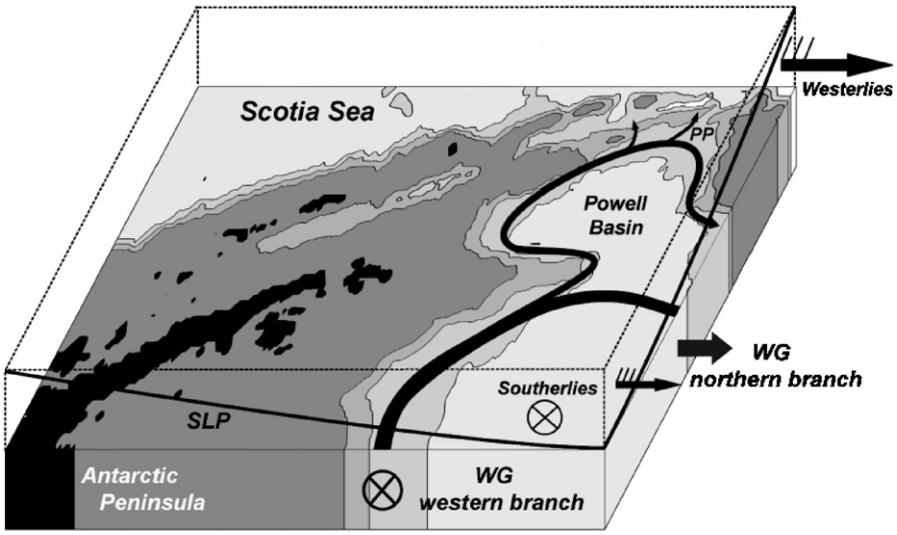

Fig. 14. Schematic diagram illustrating the favorable atmospheric conditions forcing a large-scale barotropic circulation (thick line) associated with the Weddell Gyre (WG) western and northern branches. The wind stress curl drives the WG northwestern circulation. The northward flow in the WG western branch is topographically controlled and flows cyclonically over the Powell Basin. Deeper fractions of this exit to the Southern Scotia Sea through deep gaps in the Philip Passage (thin arrows). The solid lines along the front and right sides represent the sea-level pressure (SLP), which is lowest in the southeast corner. Shading represents bottom depth (1000, 2000, and 3000 m).

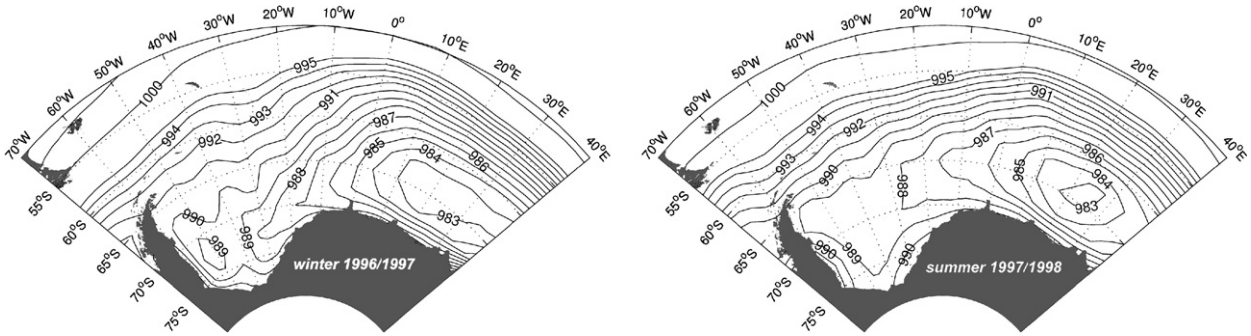

Fig. 15. Mean sea-level pressure (hPa) during austral winters (June–August) of 1996 and 1997 and austral summers (December–February) of 1996–1997 and 1997–1998.

barotropic, the northeasterly winds observed in the summer of 2001 may have led to the weakening of cyclonic circulation over the Powell Basin suggested by our inversions (Section 4.3.2.2). A schematic diagram of the proposed circulation is presented in Fig. 14. It illustrates the atmospheric conditions favorable to the development of a robust cyclonic circulation in the WG, which branches into the Powell Basin. Long-term current measurements from the northwestern boundary of the WG reported by von Gyldenfeldt et al. (2002) present relatively strong (weak) mean currents prevailing in winter (summer) and flow reversals occurring on the shelf near the tip of the Peninsula, mainly during spring and summer. Analysis of seasonal SLP distributions from NCEP/NCAR monthly means during the period of the current meter observations (May 1996–March 1998) show a westward extension of the low pressure center in the Weddell Sea during austral winter (Fig. 15). During 1997 the low-pressure center located over the WG was also intensified and displaced westward, inducing high SLP gradients in the western Weddell Sea (Fahrbach et al., 2004). This atmospheric pattern was persistent during the austral winter of 1997 (Franco, 2006) and may have been responsible for

the strong cyclonic circulation observed over the Powell Basin in August (see Gordon et al., 2001). Thus, seasonal and interannual variability of the cyclonic circulation in the northwestern WG and Powell Basin appear to be modulated by changes in the curl of the wind stress associated with changes in the location and intensity of the low-pressure center, as suggested in Fig. 14. In addition, Fahrbach et al. (2004) suggested that variations in the intensity and displacement of the WG low-pressure center affect the wind patterns in the Weddell Sea. Hence, variations in the structure and intensity of the gyre can induce variability in CDW intrusions into the WG, which would lead to variations in WDW properties. Though our Philip Passage observations from the summers of 2000 and 2001 present significant variations in WDW properties, the superimposed mesoscale variability prevents us from drawing conclusions on the possible impact of the atmospheric variability on the interannual changes of deep water properties.

6. Summary and final remarks

This study provides the first estimates of geostrophic transports through the main deep gaps in the South Scotia Ridge in the northwestern Weddell Sea using inverse methods based on quasi-synoptic observations. The WSDW exported through the deep gaps during the austral summers of 2000 and 2001 were analyzed. Implementing the inverse model with bottom triangle extrapolations and using property anomaly equations weighted by the flow estimate uncertainties, we obtained results consistent with the dominant barotropic patterns reported in the literature. West of Southern Orkney Island, over the Philip Passage, WSDW transports 0.12 ± 0.03 and 0.113 ± 0.001 Sv in the summers of 2000 and 2001, respectively. Full-depth transports through the passage were 0.84 ± 0.11 Sv in 2000 and 0.72 ± 0.06 Sv in 2001. Therefore, WSDW outflow through the Philip Passage does not present significant variations in the austral summers of 2000 and 2001. Extensive sea ice coverage during the summer of 2001 prevented the reoccupation of the stations east of South Orkney Island, over the Orkney Passage and in the region southwest of Bruce Passage. During the summer of 2000 WSDW transported 3.48 ± 1.81 Sv through the Orkney Passage and 1.20 ± 2.16 Sv through the southern Bruce Passage. Full-depth transports for these passages are 5.81 ± 3.58 and 3.39 ± 4.46 Sv, respectively. Therefore, the full-depth transport through the South Scotia Ridge during the summer of 2000 agrees with the 7 ± 6 Sv estimated by Naveira Garabato et al. (2002b), based on non-synoptic data. Mesoscale structures, warmer and saltier WDW, and colder WSDW were observed west of the South Orkney Plateau over the Philip Passage during the summer of 2001 than in 2000. The inversions suggest a sharp weakening of the barotropic cyclonic flow in the Powell Basin during this season. The observed weakening may be due to northerly and northeasterly winds associated with an atmospheric low-pressure center located west of the Antarctic Peninsula. We suggest that similar sea-level pressure variations may explain the seasonal variability in the strength of the flow along the northwestern margin of the Weddell Sea reported in 1996–1998 (von Gyldenfeldt et al., 2002).

Acknowledgments

This research was funded by Grants 49.0049/99-0 (DOVETAIL) and 55.0370/02-1 (GOAL) of the Brazilian Research Council (CNPq) and it was carried out with the aid of a grant from the Inter-American Institute for Global Change Research (IAI) CRN 2076, which is supported by the US National Science Foundation (Grant GEO-0452325). We also thank the support given by the crew of R/V Ary Rongel, the Brazilian Antarctic Program (PROANTAR) and the Ministry of the Environment (MMA). BCF was supported by a CAPES/FURG—Masters Degree Scholarship. The Brazilian cruises were conducted under an agreement between Alfred-Wegener Institut für Polar und Meeresforschung (AWI, Germany) and Fundaç ão Universidade Federal do Rio Grande (FURG, Brazil). We are grateful to E. Farhbach for providing the CTD for both cruises and to H.H. Hellmer and M. Schröder for helping to gather and process the CTD data. We thank Ricardo Matano (OSU, USA) and the anonymous reviewers for providing helpful comments on an earlier draft of the manuscript.

References

Absy, J.M., 2003. Descrição e caracterização da estrutura termohalina na região noroeste do Mar de Weddell, com ênfase na variabilidade junto ao fundo. M.Sc. Thesis, Fundaç ão Universidade Federal do Rio Grande, Rio Grande, 76pp.

Arhan, M., Heywood, K.J., King, B.A., 1999. The deep waters from the Southern ocean at the entry to the Argentine Basin. Deep-Sea Research II 46 (1–2), 475–499.

Bennett, A.F., 1992. Inverse Methods in Physical Oceanography. Cambridge University Press, Cambridge, UK, 346pp.

Bindoff, N.L., Rintoul, S.R., Massom, R., 2000. Bottom water formation and polynyas in Adélie land, Antarctica. Papers and Proceedings of the Royal Society of Tasmania 133, 51–56.

Carmack, E.C., Foster, T.D., 1975. On the flow of water out of the Weddell Sea. Deep-Sea Research 22 (11), 711–724.

Deacon, G.E.R., 1933. A general account of the hydrology of the South Atlantic Ocean. Discovery Reports 7, 171–238.

Fahrbach, E., Rohardt, G., Schröder, M., Strass, V., 1994. Transport and structure of the Weddell Gyre. Annales Geophysicae 12, 840–855.

Fahrbach, E., Rohardt, G., Scheele, N., Schröder, M., Strass, V., Wisotzki, A., 1995. Formation and discharge of deep and bottom water in the northwestern Weddell Sea. Journal of Marine Research 53, 515–538.

Fahrbach, E., Schröder, M., Klepikov, A., 1998. Circulation and water masses in the Weddell Sea. In: Physics of Ice-Covered Seas, Lecture Notes from a Summer School in Savonlinna, Finland, 6–17 June, 1994. Helsinki University Press.

Fahrbach, E., Harms, S., Rohardt, G., Schröder, M., Woodgate, R.A., 2001. Flow of bottom water in the northwestern Weddell Sea. Journal of Geophysical Research 106, 2761–2778.

Fahrbach, E., Hoppema, M., Rohardt, G., Schröder, M., Wisotzki, A., 2004. Decadal-scale variations of water mass properties in the deep Weddell Sea. Ocean Dynamics 54, 77–91.

Foldvik, A., Gammelsröd, T., Törresen, T., 1985. Circulation and water masses on the southern Weddell Sea shelf. In: Jacobs, S.S. (Ed.), Oceanology of the Antarctic Continental Shelf Antarctic Research Series, Vol. 43. American Geophysical Union, Washington, DC, pp. 5–20.

Foster, T.D., Carmack, E.C., 1976. Frontal zone mixing and Antarctic Bottom Water formation in the southern Weddell Sea. Deep-Sea Research 23 (4), 301–317.

Franco, B.C., 2006. Exportação de águas profundas na região noroeste do Mar de Weddell, Antártica: Ênfase na variabilidade temporal. M.Sc. Thesis, Fundação Universidade Federal do Rio Grande, Rio Grande do Sul, Rio Grande, 142pp.

Gammelsröd, T., Foldvik, A., Nõst, O.A., Skagsetil, Õ., Anderson, L.G., Fogelqvist, E., Olsson, K., Tanhua, T., Jones, E.P., Österhus, S., 1994. Distribution of water masses on the continental shelf in the southern Weddell Sea. In: Johannessen, O.M., Muench, R.D., Overland, J.E. (Eds.), The Polar Oceans and their Role in Shaping the Global Environment: The Nansen Centennial Volume, Vol. 85. Geophysical Monograph, AGU, Washington, pp. 959–979.

Ganachaud, A., 1999. Large scale oceanic circulation and fluxes of freshwater, heat, nutrients and oxygen. Ph.D. Thesis, Massachusetts Institute of Technology/Woods Hole Oceanographic Institution, Cambridge, MA, 267pp.

Garrett, C., Munk, W.H., 1979. Internal waves in the ocean. Annual Review of Fluid Mechanics 11, 339–369.

Georgi, D.T., 1981. Circulation and bottom waters in the southwestern South Atlantic. Deep-Sea Research 28 (9A), 959–979.

Gille, S.T., 1999. Mass, heat, and salt transport in the southeastern Pacific: a circumpolar Current inverse model. Journal of Geophysical Research 104, 5191–5209.

Gordon, A.L., 1998. Western Weddell Sea thermohaline stratification. In: Jacobs, S.S., Weiss, R.F. (Eds.), Ocean, Ice and Atmosphere: Interactions at the Antarctic Continental Margin. Antarctic Research Series, Vol. 75. American Geophysical Union, Washington DC, pp. 215–240.

Gordon, A.L., Huber, B.A., 1984. Thermohaline stratification below the Southern Ocean sea ice. Journal of Geophysical Research 89, 641–648.

Gordon, A.L., Huber, B.A., Hellmer, H.H., Field, A., 1993. Deep and bottom water of the Weddell Sea's western rim. Science 262, 95–97.

Gordon, A.L., Mensch, M., Dong, Z., Smethie Jr., W.M., de Betterncourt, J., 2000. Deep and bottom waters of the Bransfield Strait eastern and central basins. Journal of Geophysical Research 105, 11337–11346.

Gordon, A.L., Visbeck, M., Huber, B., 2001. Export of Weddell Sea deep and bottom water. Journal of Geophysical Research 106, 9005–9018.

Heywood, K.J., Naveira Garabato, A.C., Stevens, D.P., 2002. High mixing rates in the abyssal Southern Ocean. Nature 415, 1011–1014.

Jackett, D.R., McDougall, T.J., 1997. A neutral density variable for the World's Oceans. Journal of Physical Oceanography 27, 237–263.

Kalnay, E., Kanamitsu, M., Kistler, R., Collins, W., Deaven, D., Gandin, L., Iredell, M., Sha, S., White, G., Woollen, J., Zhu, Y., Chelliah, M., Ebisuzaki, W., Higgins, W., Janowiak, J., Mo, K.C., Ropelewski, C., Wang, J., Leetmaa, A., Reynolds, R., Jenne, R., Joseph, D., 1996. The NCEP/NCAR 40-year reanalysis project. Bulletin of the American Meteorological Society 77, 437–471.

LaBrecque, J.L., Rabinowitz, P.D., Brenner, C., 1981. General Bathymetric chart of the Oceans (GEBCO 5:16). Canadian Hydrographic Office, Ottawa, Canada.

Lanczos, C., 1961. Linear Differential Operators. Van Nostrand, Princeton, NJ, 564pp.

Levitus, S., Antonov, J.I., Boyer, T.B., Stephens, C., 2000. Warming of the World Ocean. Science 287, 2225–2229.

Locarnini, R.A., Whitworth III, T., Nowlin Jr., W.D., 1993. The importance of the Scotia Sea on the outflow of Weddell Sea Deep Water. Journal of Marine Research 51, 135–153.

Macdonald, A.M., 1993. Property fluxes at 30°S and their implications for the Pacific–Indian throughflow and the global heat budget. Journal of Geophysical Research 98, 6851–6868.

Mantyla, A.W., Reid, J.L., 1983. Abyssal characteristics of the World Oceans waters. Deep-Sea Research 30 (8A), 805–833.

Matano, R.P., Gordon, A.L., Muench, R.D., Palma, E.D., 2002. A numerical study of the circulation in the northwestern Weddell Sea. Deep-Sea Research II 49 (21), 4827–4841.

McIntosh, P.C., Rintoul, S.R., 1997. Do box inverse models work? Journal of Physical Oceanography 27, 291–308.

Meredith, M.P., Naveira Garabato, A.C., Steves, D.P., Heywood, K.J., Sanders, R.J., 2001. Deep and bottom waters in the eastern Scotia Sea: rapid changes in properties and circulation. Journal of Physical Oceanography 31, 2157–2168.

Morgan, P.P., 1994. Box inverse modelling with DOBOX 4.2. CSIRO Marine Laboratories Report 225, 26pp.

Muench, R.D., Gordon, A.L., 1995. Circulation and transport of water along the western Weddell Sea margin. Journal of Geophysical Research 100, 18503–18515.

Muench, R.D., Hellmer, H.H., 2002. The international DOVETAIL program. Deep-Sea Research II 49 (21), 4711–4714.

Munk, W.H., 1981. Internal waves. In: Warren, B.A., Wunsch, C. (Eds.), Evolution of Physical Oceanography, Scientific surveys in honor of Henry Stommel. MIT Press, Cambridge, MA, pp. 264–291.

Naveira Garabato, A.C., Heywood, K.J., Stevens, D.P., 2002a. Modification and pathways of Southern Ocean deep waters in the Scotia Sea. Deep-Sea Research I 49 (4), 681–705.

Naveira Garabato, A.C., McDonagh, E.L., Stevens, D.P., Heywood, K.J., Sanders, R.J., 2002b. On the export of Antarctic Bottom Water from the Weddell Sea. Deep-Sea Research II 49 (21), 4715–4742.

Naveira Garabato, A.C., Stevens, D.P., Heywood, K.J., 2003. Water mass conversion, fluxes, and mixing in the Scotia Sea diagnosed by an inverse model. Journal of Physical Oceanography 33, 2565–2587.

Naveira Garabato, A.C., Polzin, K.L., King, B.A., Heywood, K.J., Visbeck, M., 2004. Widespread intense turbulent mixing in the Southern Ocean. Science 303, 210–213.

Nowlin Jr., W.D., Zenk, W., 1988. Westward bottom currents along the margin of the South Shetland Island Arc. Deep-Sea Research 35 (2), 269–301.

Orsi, A.H., Nowlin Jr., W.D., Whitworth III, T., 1993. On the circulation and stratification of the Weddell Gyre. Deep-Sea Research I 40 (1), 169–203.

Orsi, A.H., Whitworth III, T., Nowlin Jr., W.D., 1995. On the meridional extent and fronts of the Antarctic Circumpolar Current. Deep-Sea Research I 42 (5), 641–673.

Orsi, A.H., Johnson, G.C., Bullister, J.L., 1999. Circulation, mixing, and production of Antarctic Bottom Water. Progress in Oceanography 43, 55–109.

Padman, L., Howard, S., Muench, R., 2006. Internal tide generation along the South Scotia Ridge. Deep-Sea Research II 53 (1–2), 157–171.

Reid, J.L., Lynn, R.J., 1971. On the influence of the Norwegian-Greenland and Weddell seas upon the bottom waters of the Indian and Pacific oceans. Deep-Sea Research 18, 1063–1088.

Rintoul, S.R., 1991. South Atlantic interbasin exchange. Journal of Geophysical Research 96, 2675–2692.

Rintoul, S.R., 1998. On the origin and influence of Adélie Land Bottom Water. In: Jacobs, S.S., Weiss, R.F. (Eds.), Ocean, Ice, and Atmosphere. Interactions at the Antarctic Continental Margin. Antarctic Research Series, vol. 75, pp. 151–171.

Robertson, R., Visbeck, M., Gordon, A.L., Fahrbach, E., 2002. Long-term temperature trends in deep waters of the Weddell Sea. Deep-Sea Research II 49 (21), 4791–4806.

Roemmich, D., 1981. Circulation of the Caribbean Sea: A well-resolved inverse problem. Journal of Geophysical Research 86, 7993–8005.

Roemmich, D., Wunsch, C., 1985. Two transatlantic sections: meridional circulation and heat flux in the subtropical North Atlantic Ocean. Deep-Sea Research 32 (6), 619–664.

Schodlok, M.P., Hellmer, H.H., Beckmann, A., 2002. On the transport, variability and origin of dense water masses crossing the South Scotia Ridge. Deep-Sea Research. II 49 (21), 4807–4825.

Schröder, M., Fahrbach, E., 1999. On the structure and the transport in the eastern Weddell Gyre. Deep-Sea Research II 46 (1–2), 501–527.

Schröder, M., Hellmer, H.H., Absy, J.M., 2002. On the near-bottom variability in the northwestern Weddell Sea. Deep-Sea Research.II 49 (21), 4767–4790.

Venegas, S.A., Drinkwater, M.R., 2001. Sea ice, atmosphere and upper ocean variability in the Weddell Sea, Antarctica. Journal of Geophysical Research 106, 16747–16766.

von Gyldenfeldt, A.-B., Fahrbach, E., Garcia, M.A., Schröder, M., 2002. Flow variability at the tip of the Antarctic Peninsula. Deep-Sea Research II 49 (21), 4743–4746.

Whitworth III, T., Orsi, A.H., Kim, S.-J., Nowlin Jr., W.D., Locarnini, R.A., 1998. Water masses and mixing near the Antarctic Slope Front. In: Jacobs, S.S., Weiss, R.F. (Eds.), Ocean, Ice, and Atmosphere: Interactions at the Antarctic Continental Margin. Antarctic Research Series, vol. 75, pp. 1–27.

Wunsch, C., 1977. Determining the general circulation of the oceans: A preliminary discussion. Science 196, 871–875.

Wunsch, C., 1978. The North Atlantic general circulation west of 50°W determined by inverse methods. Reviews of Geophysics and Space Physics 16, 583–620.

Wunsch, C., 1996. The ocean circulation inverse problem. Cambridge University Press, Cambridge, 437pp.

Wüst, G., 1933. Das Bodenwasser und die Gliederung der Atlantischen Tiefsee. Wissenschaftliche Ergebnisse der Deutschen Atlantischen Expedition auf dem Forschungs- und Vermessungsschiff "Meteor" 1925–1927, 6, 1–106.

Yaremchuk, M., Nechaev, D., Schröter, J., Fahrbach, E., 1998. A dynamically consistent analysis of circulation and transports in the southwestern Weddell Sea. Annales Geophysicae 16, 1024–1038.